nature metabolism

Article

https://doi.org/10.1038/s42255-026-01467-2

Fatty acids promote uncoupled respiration via ATP/ADP carriers in white adipocytes

Received: 16 September 2024

Accepted: 21 January 2026

Published online: 23 February 2026

Check for updates

Maryam Ahmadian[1,5], A. Melisa Aksu[2,5], Preetveer Dhillon[2,5], Zane J. Zerbel[2,5], Yosip Kelemen[2], Oluwafemi Gbayisomore[2], Nicolás Gómez-Banoy[2,3,4], Serena J. Chen[2] & Shannon M. Reilly[1,2]

Energy stored in adipocytes as triglycerides is mobilized via lipolysis, releasing fatty acids and glycerol into the circulation. Re-esterification of fatty acids that remain within the adipose tissue is the primary driver of adipocyte ATP consumption. Paradoxically, re-esterification suppresses respiration in lipolytic adipocytes. We previously found that STAT3 drives respiration by inhibiting re-esterification via GPAT3. Here we show that free fatty acids drive uncoupled respiration in complex with the ATP/ADP carriers. The impacts of lipolysis and re-esterification on uncoupled respiration correspond with fatty acids, not fatty acyl-CoAs or beta-oxidation. Under standard housing conditions, brown adipocyte uncoupling via uncoupling protein 1 is the dominant thermogenic pathway. However, in obese thermoneutral-adapted mice, uncoupled respiration in white adipocytes contributes to thermogenesis and cold tolerance, independent of brown adipose tissue or muscle activity. Our results suggest that uncoupled respiration in white adipocytes contributes to whole-body energy expenditure and could be a promising target for obesity treatment.

Adipocytes are essential for the maintenance of metabolic health[1,2]. Excess nutrient storage as triglycerides in adipocytes protects against ectopic lipid deposition and lipotoxicity. Stored triglycerides are hydrolysed during catabolic states such as starvation or cold exposure. Mobilization of triglycerides in the adipose tissue is prompted by catecholamine release from the sympathetic nervous system, which activates lipolysis via β-adrenergic receptor signalling. During lipolysis, fatty acid side chains are sequentially cleaved from the glycerol backbone resulting in high intracellular fatty acid flux in white adipocytes[3]. While most of these free fatty acids are released into the circulation providing fuel for other tissues, a fraction remains in the adipose tissue. How adipocytes handle this onslaught of fatty acids during active lipolysis is a fundamental question of metabolic importance.

Free fatty acids must be activated into fatty acyl-CoA to undergo either β-oxidation or esterification[4,5]. White adipocytes possess robust fatty acid esterification capacity. Re-esterification of fatty acids during lipolysis results in futile triglyceride cycling, consuming 7 ATP per cycle. During lipolysis the high rate of fatty acid efflux accelerates triglyceride cycling. The overall increase in re-esterification masks its repression in lipolytic white adipocytes[6–8]. One pathway suppressing fatty acid re-esterification is mediated by STAT3, which when serine phosphorylated in response to increased intracellular fatty acids suppresses GPAT3, the first and rate-limiting step in the glycerol lipid synthesis pathway[6]. This lipolysis-dependent inhibition of esterification correlates with increased oxidative metabolism, suggesting that elevated intracellular fatty acid levels during lipolysis drive oxidative metabolism in white adipocytes[6,9].

During lipolysis, esterification is the primary ATP-demanding pathway, and yet esterification is inversely correlated with respiratory rate, suggesting that lipolysis-driven respiration is uncoupled from

[1]Division of Metabolism and Endocrinology, Department of Medicine, University of California San Diego, La Jolla, CA, USA. [2]Weill Center for Metabolic Health, Division of Endocrinology and Metabolism, Department of Medicine, Weill Cornell Medicine, New York, NY, USA. [3]Laboratory of Molecular Metabolism, The Rockefeller University, New York, NY, USA. [4]Division of Endocrinology, Department of Medicine, Memorial Sloan Kettering Cancer Center, New York, NY, USA. [5]These authors contributed equally: Maryam Ahmadian, A. Melisa Aksu, Preetveer Dhillon, Zane J. Zerbel.
e-mail: smr4005@med.cornell.edu

ATP demand. Indeed, lipolytic activation of oxidative metabolism is associated with a decrease in mitochondrial membrane potential[9–14]. In brown adipocytes, the dissipation of the proton motive force is induced by fatty acid activation of uncoupling protein 1 (UCP1)-mediated proton leak[15]. Here we demonstrate that the ATP/ADP carrier (AAC, also known as adenine nucleotide translocase, ANT, encoded by *Slc25a4* and *Slc25a5*) is responsible for uncoupling during lipolysis in white adipocytes. Similar to UCP1, AAC uncoupling activity is activated by fatty acids[16,17]. Furthermore, we demonstrate that lipolysis-driven uncoupled respiration in white adipocytes contributes to thermogenesis and energy expenditure in obese thermoneutral-adapted mice, a physiologically relevant phenomenon impacting whole-body energy balance.

Results

Lipolysis drives oxidative metabolism in white adipocytes

We observed increased oxidative metabolism in 3T3-L1 adipocytes treated with the β-3 adrenergic receptor agonist CL-316,243 (Fig. 1a). Primary adipocyte precursor cells differentiated in vitro exhibited an even more robust increase in oxidative metabolism in response to CL-316,243 (Fig. 1b). While the maximal respiratory capacities of these adipocytes are comparable, differentiated primary adipocytes are more lipolytically active than 3T3-L1 adipocytes (Fig. 1c). Treatment with the adipose tissue triglyceride lipase (ATGL) inhibitor atglistatin blocked this increase in oxidative metabolism, suggesting it is dependent on lipolysis (Fig. 1a,b). Atglistatin treatment inhibited both stimulated and basal lipolysis in differentiated primary adipocytes (Fig. 1d,e). Basal lipolytic activity in differentiated primary adipocytes corresponded to atglistatin-sensitive oxygen consumption (Fig. 1b). The increase in lipolysis-driven oxidative metabolism and oxygen consumption was observed with a variety of lipolytic activators, including the pan β-adrenergic agonist isoproterenol, norepinephrine and the adenylyl cyclase activator forskolin (Fig. 1f,g). The induction of oxygen consumption was dose-dependent and corresponded with the rate of lipolysis (Fig. 1h–j). As expected, insulin attenuated lipolysis and the induction of oxidative metabolism (Fig. 1k,l). In summary, oxidative metabolism in differentiated primary adipocytes increases proportionally to the rate of lipolysis, consistent with previous observations in white adipocytes[6,9,11,15,18].

Intracellular fatty acid levels drive oxidative metabolism

Free fatty acids have poor aqueous solubility. In circulation they are solubilized by albumin binding. Bovine serum albumin (BSA) in cell culture media buffers free fatty acids, reducing intracellular fatty acid levels by sequestering them in the media. Without BSA in the media, fatty acids are insoluble and must be taken back up by the adipocytes (Fig. 2a). Increasing the fatty acid binding capacity in the media increases the rate of lipolysis (Fig. 2b), consistent with feedback inhibition of lipolysis by long-chain fatty acids[3,19–22]. Fatty acid sequestration by BSA in the media modulates the released fatty acid to glycerol ratio (Fig. 2c). Despite increasing lipolytic rates, BSA dose-dependently reduces oxidative metabolism during lipolytic stimulation (Fig. 2d), demonstrating that intracellular fatty acid levels drive respiration. Notably, lipolysis-driven oxidative metabolism, while attenuated, still occurs in the presence of high BSA concentrations, suggesting that it is not an artifact of cell culture conditions with insufficient fatty acid binding capacity.

Fatty acid re-esterification suppresses oxidative metabolism

Lipolysis-driven oxidative metabolism in white adipocytes is promoted by STAT3-mediated inhibition of GPAT3, the first and rate-limiting step in glycerol lipid synthesis[6]. We confirmed that *Stat3* knockout (KO) adipocytes treated with CL-316,243 exhibited lower lipolysis-driven oxidative metabolism compared with wild-type (WT) adipocytes, without changing the rate of lipolysis (Extended Data Fig. 1). To further examine the interplay between re-esterification and oxidative metabolism, we inhibited triglyceride synthesis with the diacylglycerol acyltransferase 1 (DGAT1) inhibitor PF-04620110, effectively blocking triglyceride cycling[23–25]. Interestingly, inhibition of DGAT1 increased adipocyte oxygen consumption (Fig. 2e). Furthermore, eliminating ATP demand for fatty acid activation with the ASCL inhibitor triacsin C also increased adipocyte oxygen consumption (Fig. 2f). Fatty acid oxidation is also dependant on ASCL-mediated activation of free fatty acids. To specifically investigate the impact of mitochondrial β-oxidation we utilized etomoxir to inhibit the carnitine shuttle required to import fatty acyl-CoAs into the mitochondria. Pretreatment with etomoxir did not suppress the rate of oxidative metabolism, indicating that mitochondrial fatty acid oxidation is not required (Fig. 2g). Thus, neither ATP demand for triglyceride cycling nor β-oxidation drive oxidative metabolism in lipolytic adipocytes. Rather, these results suggest that free fatty acids drive respiration. Indeed, sequestration of excess fatty acids by BSA in the media pre-empts the positive impact of DGAT1 inhibition on oxidative metabolism (Fig. 2h). Importantly, DGAT1 inhibition did not affect the rate of lipolysis as determined by glycerol release rate (Fig. 2i). Consistent with supressed triglyceride synthesis, slightly more fatty acids were released during stimulated lipolysis in the presence of the DGAT1 inhibitor (Fig. 2j). Triacsin C also did not impact the rate of lipolysis (Fig. 2k,l).

Adipocyte mitochondria are uncoupled by fatty acids during lipolysis

As ATP demand for triglyceride synthesis does not drive respiration in lipolytic adipocytes, we investigated mitochondrial uncoupling, which is characterized by loss of membrane potential despite high oxygen consumption. Mitochondrial membrane potential decreased drastically upon lipolytic activation, as determined by staining with the membrane potential-dependent dye tetramethylrhodamine methyl ester perchlorate (TMRM), while the membrane potential-independent dye, MitoTracker Green, remained stable (Fig. 3a and Extended Data Fig. 2a–c). Another membrane potential-dependent dye, JC-10, also indicated mitochondrial depolarization in lipolytic adipocytes with a reduction in the bound (red) intensity and an increase in the unbound (green) intensity relative to the vehicle controls (Extended Data Fig. 2d–g).

The loss of membrane potential was blocked by either ATGL knockdown or inhibition (Fig. 3b,c). Although slower than stimulated cells, vehicle control cells also lost membrane potential over time in an ATGL-dependent manner. Concurrent with the dissipation of membrane potential, oxygen consumption rates increased (Fig. 3d). This rapid dissipation of the proton motive force despite electron transport chain activity is suggestive of uncoupled respiration. Norepinephrine also induced a lipolysis-dependent loss of mitochondrial membrane potential (Fig. 3e). Sequestration of fatty acids by BSA in the media attenuated the loss of membrane potential and reduced the rate of oxygen consumption upon stimulation with norepinephrine (Fig. 3f,g). BSA similarly attenuated depolarization in response to CL-316,243 (Fig. 3h). While free fatty acids can flip through membranes to enter the mitochondria, long-chain fatty acyl-CoAs depend on the carnitine shuttle to enter the mitochondria. Inhibition of CPT1 with etomoxir did not block mitochondrial depolarization, indicating that mitochondrial import of fatty acyl-CoAs is dispensable (Fig. 3i). Inhibition of esterification by STAT3, triacsin C or PF-04620110 increased mitochondrial depolarization in accordance with induction of oxidative metabolism (Extended Data Fig. 3). These data suggest that elevated intracellular free fatty acids mediate mitochondrial depolarization in lipolytic adipocytes.

Lipolysis-driven respiration is oligomycin insensitive

During coupled respiration, ATP synthase utilizes the proton motive force to drive ATP production. To investigate the role of ATP synthase in the loss of proton motive force, we pretreated cells with oligomycin

https://doi.org/10.1038/s42255-026-01467-2

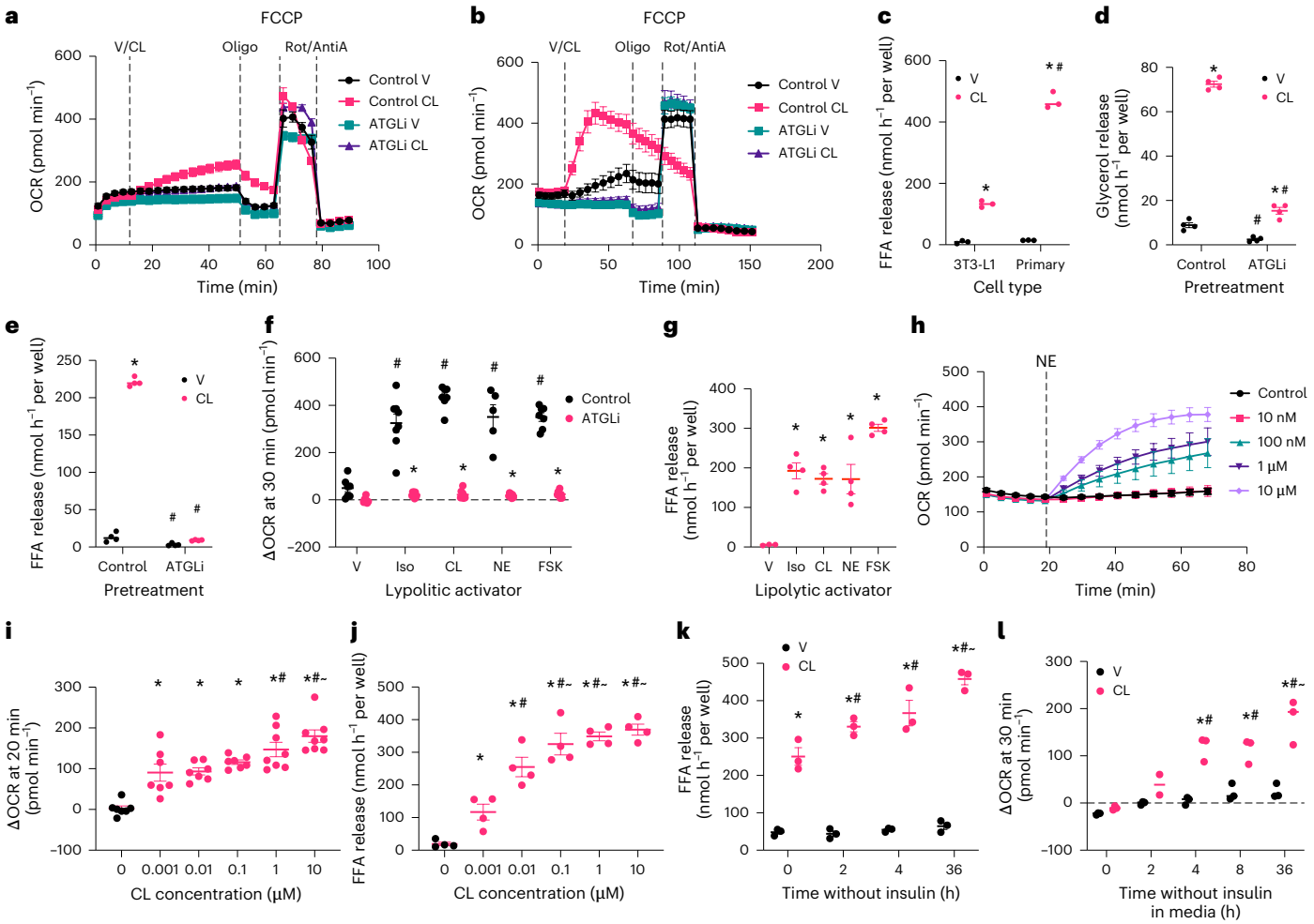

Fig. 1 | Lipolysis-driven oxidative metabolism in white adipocytes. **a**,**b**, Oxygen consumption rate (OCR) in differentiated 3T3-L1 adipocytes (**a**) and male primary adipocytes (**b**) pretreated with 50 μM atglistatin (ATGL inhibitor, ATGLi) or control and stimulated with CL-316,243 (CL), 10 μM in **a** and 100 nM in **b**; $P < 0.05$ between all groups throughout vehicle (V) and CL treatment; $n = 6$ wells (**a**) and $n = 12$ wells (**b**). **c**, Rate of free fatty acid (FFA) release from 3T3-L1 and male primary adipocytes treated with V or 10 μM CL, $n = 3$ wells; $^{*}P < 0.05$ V versus CL; $^{\#}P < 0.05$ primary versus 3T3-L1. **d**,**e**, Glycerol (**d**) and FFA (**e**) release from male primary adipocytes pretreated with 50 μM ATGLi or V and stimulated with CL or V, $n = 4$ wells; $^{*}P < 0.05$ V versus CL; $^{\#}P < 0.05$ control versus ATGLi. **f**, Change in OCR in male primary adipocytes pretreated with 50 μM ATGLi or V from baseline to 30 min after stimulation with V, 1 μM isoproterenol (Iso), 500 nM CL, 10 μM norepinephrine (NE) or 10 μM forskolin (FSK), $n = 7$ wells, except FSK control $n = 5$ wells; $^{*}P < 0.05$ control versus ATGLi; $^{\#}P < 0.05$ versus V. **g**, Rate of FFA release from female primary adipocytes, $n = 4$ wells; $^{*}P < 0.05$ versus V. **h**, OCR in female primary adipocytes at baseline and after NE stimulation, $n = 6$ wells; $P < 0.05$ for all comparisons except 10 nM NE versus control. **i**,**j**, Change in OCR (**i**) from baseline to 20 min after CL stimulation and rate of FFA release (**j**) from male primary adipocytes, $n = 7$ wells except 1 and 10 μM CL $n = 8$ wells (**i**) and 4 wells (**j**); $^{*}P < 0.05$ versus control; $^{\#}P < 0.05$ versus 1 nM CL; $^{\sim}P < 0.05$ versus 10 nM CL. **k**,**l**, Rate of FFA release (**k**) and change in OCR (**l**) from baseline to 30 min after stimulation with CL or V in male primary adipocytes following varying durations in insulin-free media, $n = 4$ wells (**k**) and 3 wells (**l**); $^{*}P < 0.05$ V versus CL; $^{\#}P < 0.05$ versus 0 h; $^{\sim}P < 0.05$ versus 2 h. Data are mean ± s.e.m. Statistical significance was determined by one-way ANOVA (**g**,**i**,**j**) or two-way ANOVA (**a**–**f**,**h**,**k**,**l**) with Holm–Šidák correction; exact P values are provided in the Source Data[68]. AntiA, antimycin A; Oligo, oligomycin; Rot, rotenone.

to inhibit ATP synthesis. Inhibition of ATP synthase slowed the loss of membrane potential (Fig. 3j). Pretreatment with oligomycin also reduced the rate of lipolysis (Fig. 3k,l), as previously observed[26]. Thus, it is not clear whether ATP synthesis contributes to the loss of membrane potential or whether the reduction in fatty acid load slowed the loss of membrane potential. Nevertheless, substantial membrane depolarization was observed in the presence of oligomycin, strongly indicating a proton leak and uncoupled respiration (Fig. 3j). We also investigated the effect of oligomycin pretreatment on lipolysis-driven oxidative metabolism. As expected, oligomycin reduced baseline oxygen consumption by blocking coupled respiration; however, oxygen consumption rapidly increased upon CL-316,243 stimulation in the oligomycin-treated adipocytes, catching up with the CL-316,243-treated control adipocytes (Fig. 3m). This suggests that ATP utilization is not the driving force behind the increase in oxidative metabolism, but rather a proton-leak-dependent reduction in membrane potential facilitates electron transport, increasing oxygen consumption and upstream substrate utilization.

Lipolysis-driven respiration is not uncoupled by UCP1

In brown adipocytes, uncoupled respiration occurs due to activation of UCP1 by fatty acids[27–30]. UCP1 expression in our differentiated primary adipocytes was undetectable (Extended Data Fig. 4a–c). Nevertheless, we investigated the impact of lentiviral-mediated UCP1 knockdown in the differentiated primary adipocytes. Efficacy of the knockdown was validated by western blot in differentiated primary brown adipocytes and by quantitative PCR in the white adipocytes (Extended Data Fig. 4d,e). UCP1 knockdown did not attenuate the loss of mitochondrial membrane potential in lipolytic white adipocytes (Extended Data Fig. 4f). These findings are consistent with previous

https://doi.org/10.1038/s42255-026-01467-2

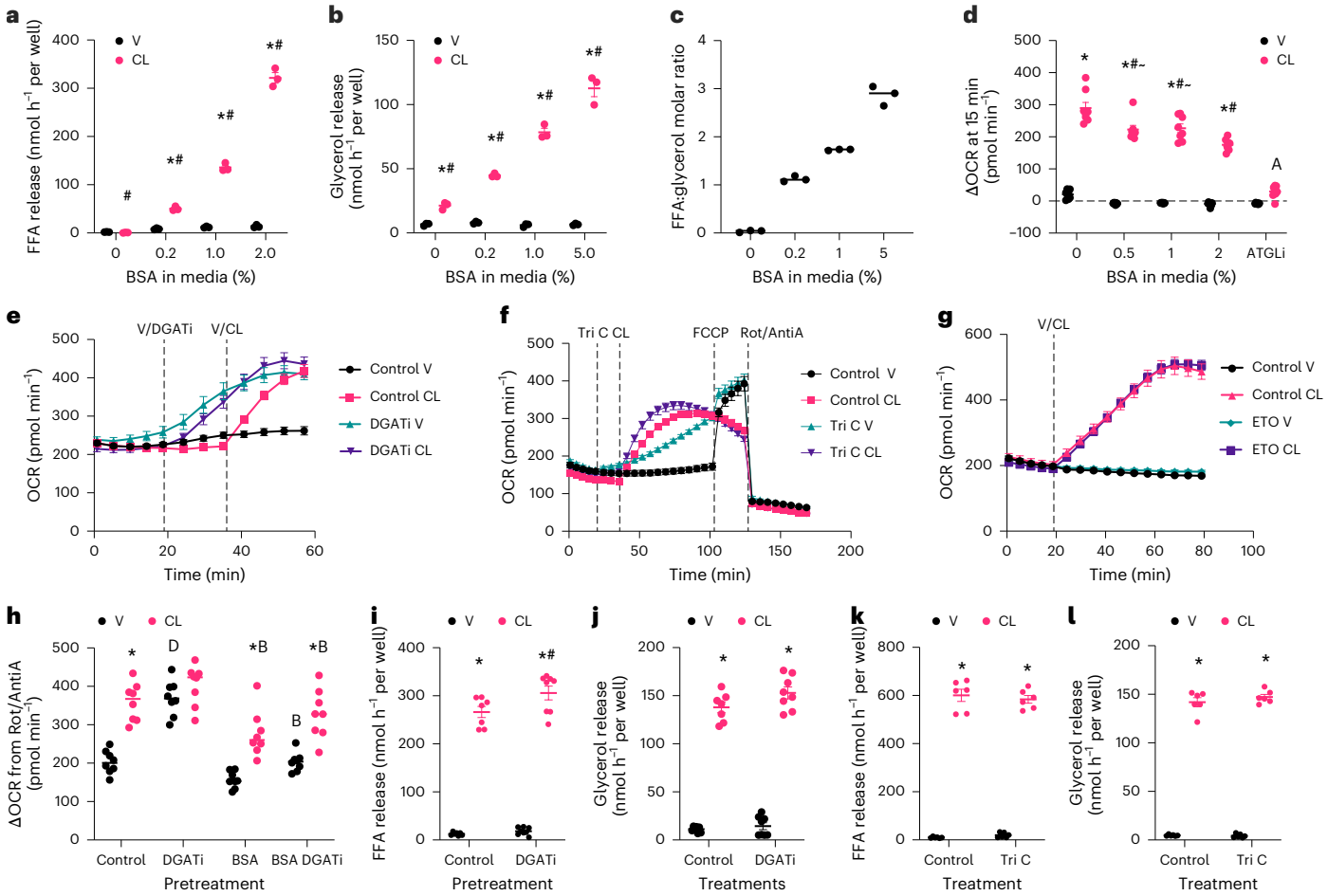

Fig. 2 | Fatty acid esterification antagonizes oxidative metabolism. a,**b**, Rate of FFA (**a**) and glycerol (**b**) release in male primary adipocytes treated with V or 100 nM CL in media containing varying concentrations of BSA, $n = 3$ wells; $^{*}P < 0.05$ CL versus V; $^{\#}P < 0.0001$ versus all other BSA concentrations. **c**, Ratio of fatty acid to glycerol release derived from **a** and **b**; all BSA concentrations significantly different from each other, $P < 0.01$, $n = 3$ wells. **d**, Change in OCR from baseline to 30 min after stimulation with CL or V in female primary adipocytes cultured in media containing varying concentrations of BSA or treated with 50 µM ATGLi in the absence of BSA, $n = 8$ wells; $^{*}P < 0.0001$ V versus CL; $^{\#}P < 0.0001$ versus 0% BSA; $^{-}P < 0.001$ versus 2% BSA; $^{A}P < 0.0001$ ATGLi versus all BSA concentrations. **e**, OCR in female primary adipocytes with port A injection of 10 µM PF-04620110 (DGAT inhibitor, DGATi) or V and port B injection of 50 nM CL or V at indicated time points, $n = 8$ wells; $P < 0.05$ for control V versus control CL after 35 min; control V versus DGATi V after 25 min; control CL versus DGATi CL after 20 min. **f**, OCR in female primary adipocytes with port A injection of 5 µM triacsin C or V and port B injection of CL or V at indicated time points, $n = 6$ wells; $P < 0.05$ for control V versus control CL from 10 min; control CL versus CL triacsin C from 35 to 80 min; control V versus V triacsin C from 40 min; V triacsin C versus CL triacsin C from 45 to 100 min. **g**, OCR in female primary adipocytes pretreated with 5 µM etomoxir (ETO) or control and stimulated with 10 nM CL or V, $n = 8$ wells; $P < 0.0001$ V versus CL for control and ETO after 25 min. **h**, Background-subtracted OCR after 30 min of DGATi treatment and 15 min of CL stimulation in the presence or absence of 2% BSA, $n = 8$ wells; $^{*}P < 0.0001$ V versus CL; $^{D}P < 0.0001$ control V versus DGATi V; $^{B}P < 0.01$ control versus BSA. **i**,**j**, Rate of FFA (**i**) and glycerol (**j**) release in female primary adipocytes treated with V or CL following pretreatment with DGATi or V, $n = 7$ control wells and 8 DGATi wells; $^{*}P < 0.0001$ V versus CL; $^{\#}P < 0.01$ control versus DGATi. **k**,**l**, Rate of FFA (**k**) and glycerol (**l**) release in female primary adipocytes treated with V or CL in the presence of 5 µM triacsin C or V, $n = 6$ wells; $^{*}P < 0.0001$ V versus CL. Data are mean ± s.e.m. Statistical significance was determined by one-way ANOVA (**c**) or two-way ANOVA (**a**,**b**,**d**–**l**) with Holm–Šidák correction; exact P values are provided in the Source Data[68]. Tri C, triacsin C.

reports that fatty acid-mediated uncoupling in lipolytic white adipocytes is independent of UCP1[15].

Opening of the permeability transition pore cannot account for the proton leak

The permeability transition pore (PTP) is a large multiprotein complex in the mitochondrial inner membrane that is defined by the presence of cyclophilin D[31–33]. PTP opening can result in cytochrome C release, mitochondrial swelling and cell death[34]. However, transient opening of the PTP also occurs physiologically[35,36], and has been proposed as a mechanism of uncoupling in lipolytic white adipocytes[9]. Inhibition of cyclophilin D with cyclosporin A (CSA)[37] attenuated the loss of membrane potential and the increase in lipolysis-driven oxidative metabolism but did not impact the rate of lipolysis (Extended Data Fig. 5). Although significant, the effect of CSA was small, and membrane potential dropped while oxygen consumption increased, suggesting that PTP opening is not the primary mechanism mediating mitochondrial uncoupling in lipolytic white adipocytes.

Lipolysis-driven uncoupling is dependent on AAC activity

The AACs play an essential role in coupled respiration, exporting ATP synthesized in the matrix. Interestingly, AACs have also been implicated in proton leakage and uncoupled respiration[16,17,38–47]. Similar to UCP1, AAC nucleotide binding can be outcompeted by fatty acids, leading to dissipation of the proton motive force[16,17]. Given that lipolysis-driven uncoupling appears to be mediated by fatty acids, we investigated the impact of inhibiting AAC with bongkrekic acid (BKA)[48]. Treatment with BKA blocked membrane depolarization (Fig. 4a). Importantly, BKA did not impact the rate of lipolysis (Fig. 4b,c). Since AAC activity is required to provide ADP for ATP synthesis, BKA inhibited basal

https://doi.org/10.1038/s42255-026-01467-2

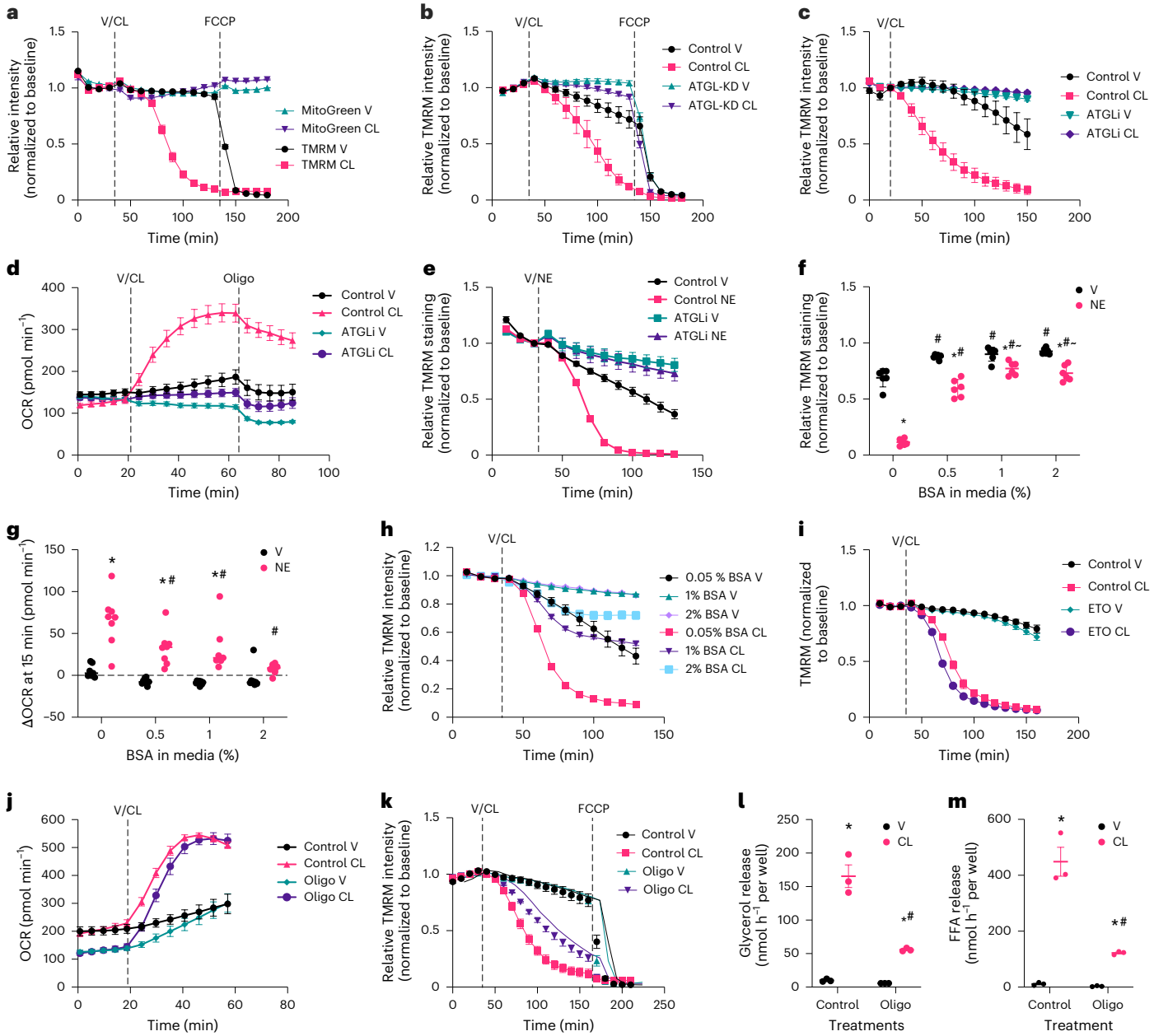

Fig. 3 | Dissipation of proton motive force during lipolysis. a, Baseline-normalized TMRM and MitoTracker Green (MitoGreen) fluorescence in female primary adipocytes stimulated with 100 nM CL, $n = 6$ wells, MitoGreen V versus CL not significant, TMRM V versus CL $P < 0.0001$, **b**, Baseline-normalized TMRM fluorescence in ATGL knockdown (KD) and control male primary adipocytes stimulated with CL or V (V $n = 6$ wells; $P < 0.05$ control V versus control CL and control CL versus ATGL-KD CL from 70 min; control V versus ATGL-KD V from 80 min; ATGL-KD V versus ATGL-KD CL from 120 min, no differences after 30 min of FCCP. **c**, Baseline-normalized TMRM fluorescence in male primary adipocytes pretreated with 50 µM ATGLi or control and stimulated with CL or V. $n = 6$ wells; $P < 0.05$ for control V versus control CL and control CL versus ATGLi CL after 40 min; control V versus ATGLi V after 120 min. **d**, OCR in male primary adipocytes pretreated with ATGLi or control and stimulated with CL or V. $n = 8$ ATGLi, 6 control V and 7 control CL wells; $P < 0.05$ control V versus control CL and control CL versus ATGLi CL after 30 min; control V versus ATGLi V after 40 min; ATGLi V versus ATGLi CL after 60 min. **e**, Baseline-normalized TMRM fluorescence in male primary adipocytes pretreated with ATGLi or control and stimulated with 10 µM NE or V. $n = 6$ wells; $P < 0.05$ for control V versus control NE, control V versus ATGLi V and control NE versus ATGLi NE after 60 min. **f**, Baseline-normalized TMRM fluorescence in male primary adipocytes 50 min after stimulation with NE or V across increasing BSA concentrations. $n = 6$ wells; $^{*}P < 0.001$ V versus NE; $^{\#}P < 0.0001$ versus control; $^{\sim}P < 0.001$ versus 0.5% BSA. **g**, Change in OCR from baseline to 15 min after NE or V stimulation across increasing BSA concentrations. $n = 8$ wells, except control V and 1% BSA NE $n = 7$ wells; $^{*}P < 0.01$ V versus NE; $^{\#}P < 0.01$ BSA versus control. **h**, Baseline-normalized TMRM fluorescence in male primary adipocytes stimulated with CL or V across 0.05–2% BSA. $n = 6$ wells; $P < 0.0001$ for V versus CL at all BSA concentrations and between BSA conditions except 1% versus 2% BSA V. **i**, Baseline-normalized TMRM fluorescence in male primary adipocytes pretreated with 5 µM ETO and stimulated with CL. $n = 6$ wells; $P < 0.05$ for control V versus control CL and ETO V versus ETO CL from 60 min; control CL versus ETO CL from 60 to 110 min; control V versus ETO V from 150 min. **j**, OCR in male primary adipocytes pretreated with 2 µM Oligo or control and stimulated with CL or V. $n = 8$ wells, except control V $n = 6$ wells; $P < 0.05$ for control V versus Oligo V and control CL versus Oligo CL from baseline to 35 min; V versus CL after 25 min. **k**, Baseline-normalized TMRM fluorescence in female primary adipocytes pretreated with Oligo and stimulated with CL. $n = 6$ wells; $P < 0.05$ for control V versus control CL after 60 min; Oligo V versus Oligo CL and control CL versus Oligo CL from 70 min; no differences after FCCP. **l**,**m**, Glycerol (**l**) and FFA (**m**) release from female primary adipocytes pretreated with Oligo and stimulated with CL. $n = 3$ wells; $^{*}P < 0.01$ V versus CL; $^{\#}P < 0.0001$ Oligo CL versus control CL. Data are mean ± s.e.m. Statistical significance was determined by two-way ANOVA with Holm–Šidák correction; exact P values are provided in the Source Data[68].

oxygen consumption to the same extent as oligomycin (Fig. 4d). However, upon lipolytic stimulation, BKA treatment blocked the increase in oxygen consumption (Fig. 4d). In the presence of oligomycin, BKA reduced lipolysis-stimulated uncoupled respiration (Fig. 4e). The effect of BKA to attenuate the induction of oxidative metabolism was dose-dependent (Fig. 4f). BKA efficiently blocked the loss of mitochondrial membrane potential at all concentrations tested (Fig. 4g). These data suggest that fatty acid binding to AAC is responsible for the proton leak that leads to the loss of mitochondrial membrane potential and drives oxidative metabolism.

Mice express three of the four AAC isoforms; AAC1 and AAC2 are somatic, while AAC4 expression is limited to the testis[49–51] (Extended Data Fig. 6). Adipocytes primarily express AAC2 (*Slc25a5*). AAC1 (*Slc25a4*)—highly expressed in heart and skeletal muscle—is also expressed in adipocytes but at lower levels. While AAC2 is detectable by western blot in whole-cell primary adipocyte lysates, AAC1 was not detected (Extended Data Fig. 4c). To further examine the roll of AACs in adipocytes, we utilized a lentivirus with puromycin selection to knock down AAC2. We achieved over 85% reduction in *Slc25a5* transcript level in the primary adipocytes, with no compensatory *Slc25a4* expression (Fig. 4h). Differentiation efficiency was not impacted by the knockdown and expression of the β-3 adrenergic receptor, *Adrb3*, was the same (Fig. 4h). AAC2 protein levels in the mitochondria were effectively reduced in the knockdown cells as compared with the control virus-treated cells (Fig. 4i). Knockdown of AAC2 reduced basal metabolic rate in the adipocytes and blunted lipolysis-induced respiration (Fig. 4j). AAC2 knockdown also blocked mitochondrial depolarization upon lipolytic stimulation (Fig. 4k). Consistent with low AAC1 expression, AAC1 knockdown did not significantly impact lipolysis-driven respiration (Fig. 4l). The effect of AAC2 was comparable to BKA treatment, and the two interventions were not additive (Fig. 4l). AAC2 knockdown blocked uncoupled respiration and loss of mitochondrial membrane potential in oligomycin-pretreated cells (Fig. 4m,n). Together, these data support AAC-mediated uncoupling in lipolytic white adipocytes.

Is uncoupled respiration in lipolytic white adipocytes thermogenic in vivo?

White adipocyte lipolysis fuels muscle shivering and brown fat thermogenesis[52–54], making it challenging to determine which tissue is the source of the thermogenic response to lipolysis in vivo. Adipocyte-specific *Stat3* knockout (SAKO) mice have a normal lipolytic response despite the defect in lipolysis-driven oxidative metabolism in adipocytes[6]. Thus, these animals are an ideal model in which to evaluate the impact of white adipocyte respiration without confounding effects of lipolysis on other thermogenic tissues. First, we investigated cold tolerance in normal-diet-fed, room temperature-housed mice. Under these conditions the thermogenic response is dominated by brown adipose tissue[55–59]. Cold tolerance and energy expenditure at both 22 °C and 5 °C were the same in the normal-diet-fed SAKO mice and floxed littermate cre-negative controls (SAWT) (Extended Data Fig. 7a–e). These results indicate that brown fat thermogenesis is not impacted by the loss of STAT3. However, when placed on a high-fat diet (HFD), SAKO mice were cold-sensitive as compared with their littermate controls (Fig. 5a).

To focus on the metabolic contributions of white adipocytes, we adapted the HFD-fed mice to thermoneutrality, inactivating their brown adipose tissue. The obese thermoneutral-adapted SAKO mice had increased body weight due to increased adiposity relative to littermate controls (Fig. 5b,c), as was previously observed in diet-induced obese mice housed at room temperature[6]. The cold sensitivity of the SAKO mice was enhanced by thermoneutral adaptation, resulting in a survival defect in the SAKO mice ($P = 0.003$) (Fig. 5d). During acute cold exposure, oxygen consumption initially increased in both genotypes, likely due to shivering (Fig. 5e). However, over time the SAKO mice failed to maintain this increased oxidative rate and the oxygen consumption dropped lower than in SAWT controls. The same pattern was observed in carbon dioxide production (Fig. 5f). No differences in respiratory exchange ratio, activity or food intake were observed (Extended Data Fig. 7f–h). Taken together, these data indicate that obese thermoneutral-adapted SAKO mice exhibit increased sensitivity to acute cold exposure, failing to mount the respiratory response required for survival in these conditions.

To determine whether the defect in cold tolerance in the SAKO mice was related to UCP1 activity, we measured its expression in brown fat and inguinal white adipose tissue. Protein levels were measured in mitochondrial fractions from adipose tissues. UCP1 protein was readily detectable in brown fat but not in inguinal white adipose tissue mitochondria from obese thermoneutral-adapted mice; expression was the same across genotypes (Extended Data Fig. 7i). Inguinal *Ucp1* messenger RNA expression was more than 100-fold lower than expression in brown fat but was not impacted by genotype (Extended Data Fig. 7j). Interestingly, AAC2 protein levels and mRNA were similar in brown and white fat (Extended Data Fig. 7i,k), suggesting that the mitochondria from these two cell types have similar potential for UCP1-independent respiration. The expression of *Gpr3* has been previously observed to be increased in response to lipolytic activation and to promote adipocyte thermogenesis[60]. Consistent with equal lipolytic response in the SAWT and SAKO mice, no differences in *Gpr3* expression were observed between genotypes (Extended Data Fig. 7l).

STAT3 is not required in brown adipocytes for thermogenesis

In the SAKO mice, *Adipoq*-CRE knocks out *Stat3* in all adipocytes. To specifically investigate the contribution of classic thermogenic adipocytes, we utilized a *Ucp1*-promoter-driven CRE to knock *Stat3* out in brown adipocytes (SBKO mice). Similar to SAKO mice, normal-diet, room temperature-housed SBKO mice exhibited no defect in cold-induced energy expenditure (Extended Data Fig. 8a,b). However, while obese thermoneutral-adapted SAKO mice exhibited cold sensitivity, SBKO mice have normal cold tolerance and energy expenditure (Extended Data Fig. 8c–f). Obese thermoneutral-adapted SBKO mice did not exhibit the increase in adiposity observed in SAKO mice (Fig. 5g). To compare the SAKO and SBKO phenotypes, we generated a cohort composed of both genotypes and their corresponding littermate controls. In an acute cold tolerance test, the SAWT and SBWT control mice defended their core temperature similarly, while the core temperature of the SAKO mice dropped significantly lower than that of the SAWT (Fig. 5h). Furthermore, SBKO mice did not exhibit the survival defect as compared with WT controls as was observed in SAKO mice (Fig. 5i). During acute cold exposure, oxygen consumption in SBKO mice was not significantly different from their SBWT littermate controls, while oxygen consumption in SAKO mice was significantly lower than in both SAWT and SBKO mice (Fig. 5j). Carbon dioxide production in the SBKO mice dropped lower than in the SBWT controls; however, the rate in the SAKO mice dropped earlier and was significantly lower than in the SBKO mice (Fig. 5k). Additionally, there were no significant differences in thermogenic gene expression in inguinal or epididymal adipose tissue (Extended Data Fig. 9). Overall, these data indicate that *Stat3* KO in white adipocytes causes increased sensitivity to cold in obese thermoneutral-adapted mice, which is associated with a defect in energy expenditure in the cold. Also, KO of *Stat3* in brown adipocytes has no impact on thermogenesis regardless of body composition or housing temperature.

Lipolysis-driven thermogenesis is independent of muscle activity

Physical activity generates heat, and shivering contributes to energy expenditure during acute cold exposure. To isolate the effect of lipolysis-driven uncoupled respiration on thermogenesis, we blocked muscle activity with pentobarbital in obese thermoneutral-adapted mice. Even at an ambient temperature of 30 °C, when mice were immobilized with pentobarbital their core body temperature declined rapidly

https://doi.org/10.1038/s42255-026-01467-2

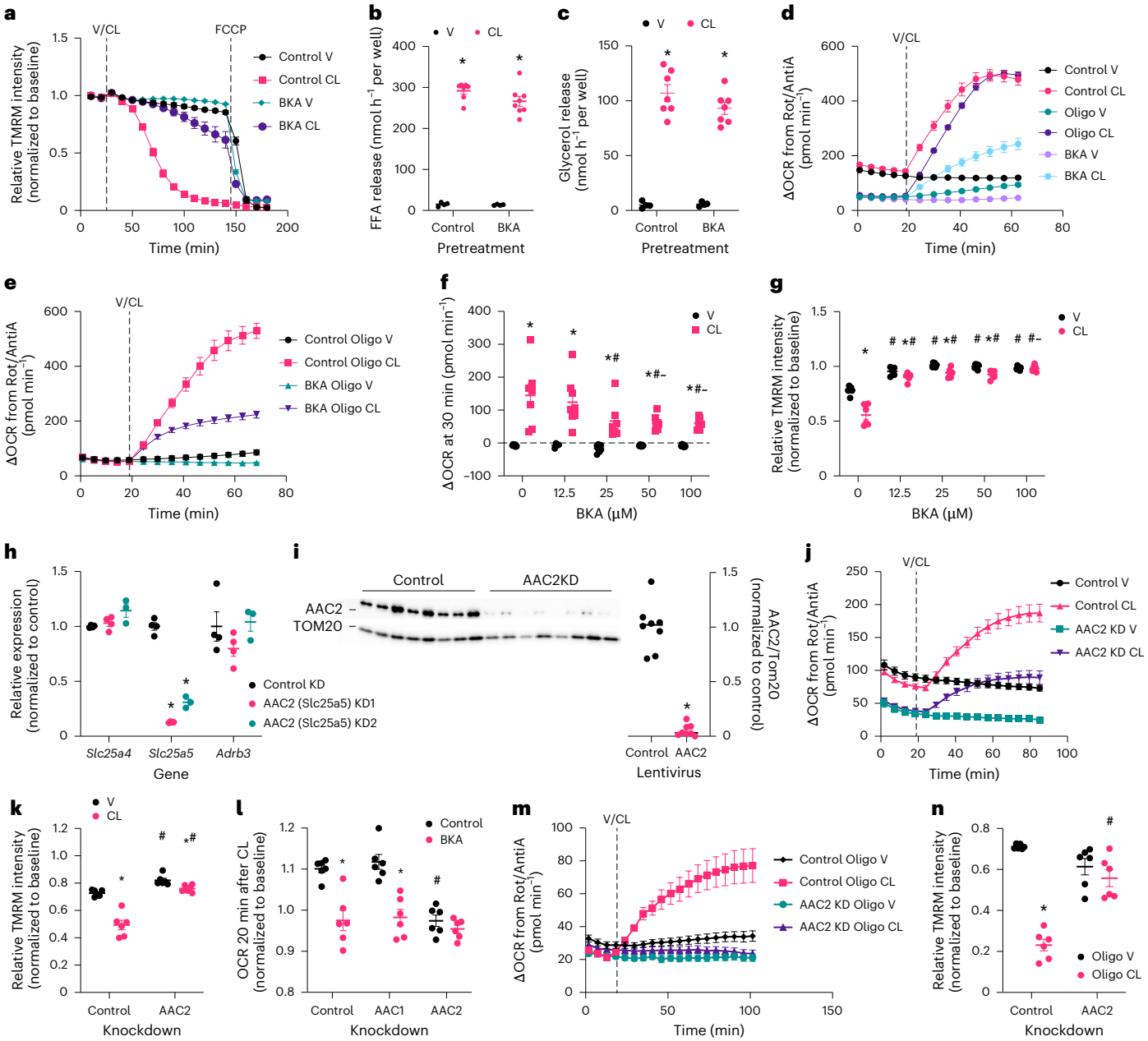

Fig. 4 | Fatty acids promote uncoupling via AAC in white adipocytes. **a**, Baseline-normalized TMRM fluorescence in female primary adipocytes pretreated with 100 μM BKA or V and stimulated with 100 nM CL followed by FCCP at indicated time points, $n = 6$ wells; $P < 0.05$ for control V versus control CL after 60 min; control V versus V BKA after 90 min; control CL versus CL BKA after 50 min; BKA V versus BKA CL after 80 min; no differences after 30 min of FCCP. **b**,**c**, Rate of FFA (**b**) and glycerol (**c**) release in male primary adipocytes pretreated with V or 100 μM BKA and stimulated with CL, $n = 4$ V wells and 7 CL wells; $^{*}P < 0.0001$ V versus CL. **d**, Background-subtracted OCR in male primary adipocytes pretreated with 100 μM BKA, 2 μM Oligo or control and stimulated with 50 nM CL via port A, $n = 7$ control and Oligo wells and $n = 8$ BKA wells; $P < 0.05$ for control V versus Oligo V from 0 to 60 min; control CL versus Oligo CL from 0 to 50 min; control versus BKA for V and CL at all time points; V versus CL for control, Oligo and BKA after 20 min. **e**, Background-subtracted OCR in female primary adipocytes pretreated with 2 μM Oligo with or without 100 μM BKA and stimulated with V or 50 nM CL, $n = 8$ wells; $P < 0.05$ V versus CL in all groups and control CL versus BKA CL after 20 min. **f**, Change in OCR from baseline to 30 min after stimulation with 50 nM CL or V in female primary adipocytes pretreated with increasing concentrations of BKA, $n = 7$ wells except 12.5 μM BKA V $n = 4$ wells; $^{*}P < 0.01$ V versus CL; $^{\#}P < 0.05$ versus no BKA control; $^{\sim}P < 0.05$ versus 12.5 μM BKA. **g**, Baseline-normalized TMRM fluorescence in male primary adipocytes pretreated with BKA and stimulated with V or 50 nM CL, $n = 6$ wells; $^{*}P < 0.05$ V versus CL; $^{\#}P < 0.0001$ versus no BKA control; $^{\sim}P < 0.05$ versus 12.5 μM BKA. **h**, Gene expression in AAC2 KD and control male primary adipocytes, $n = 4$ wells except AAC2 KD2 $n = 3$ wells; $^{*}P < 0.0001$ versus control. **i**, Western blot and quantification of mitochondrial fractions from male primary adipocytes with molecular weight markers indicated, $n = 8$ wells; $^{*}P = 0.002$. **j**, Background-subtracted OCR in AAC2 KD and control female primary adipocytes, $n = 8$ wells; $P < 0.05$ control versus AAC2 KD at all time points and control V versus CL from 30 min. **k**, Baseline-normalized TMRM fluorescence in AAC2 KD and control female primary adipocytes 40 min after stimulation, $n = 6$ wells; $^{*}P < 0.05$ V versus CL, control < 0.0001 and AAC2 KD = 0.047; $^{\#}P < 0.05$ control versus KD, V = 0.004 and CL < 0.0001. **l**, Baseline-normalized OCR 15 min after CL stimulation in AAC1 KD, AAC2 KD and control male primary adipocytes pretreated with 25 μM BKA or V, $n = 6$ wells; $^{*}P < 0.0001$ V versus BKA; $^{\#}P < 0.0001$ control versus KD. **m**, Background-subtracted OCR in AAC2 KD and control male primary adipocytes pretreated with 2 μM Oligo and stimulated with 10 nM CL or V, $n = 8$ V wells and 7 CL wells; $P < 0.05$ Oligo V versus Oligo CL and Oligo CL versus Oligo AAC2 KD CL from 30 min. **n**, Baseline-normalized TMRM fluorescence in AAC2 KD and control male primary adipocytes pretreated with 2 μM Oligo and stimulated with 10 nM CL or V for 40 min, $n = 6$ wells; $^{*}P < 0.0001$ V versus CL; $^{\#}P < 0.0001$ control versus KD. Data are mean ± s.e.m. Statistical significance was determined by two-way ANOVA with Holm–Šidák correction (**a**–**h**,**j**–**m**) or non-parametric two-tailed *t*-test (**i**); exact *P* values are provided in the Source Data[68].

https://doi.org/10.1038/s42255-026-01467-2

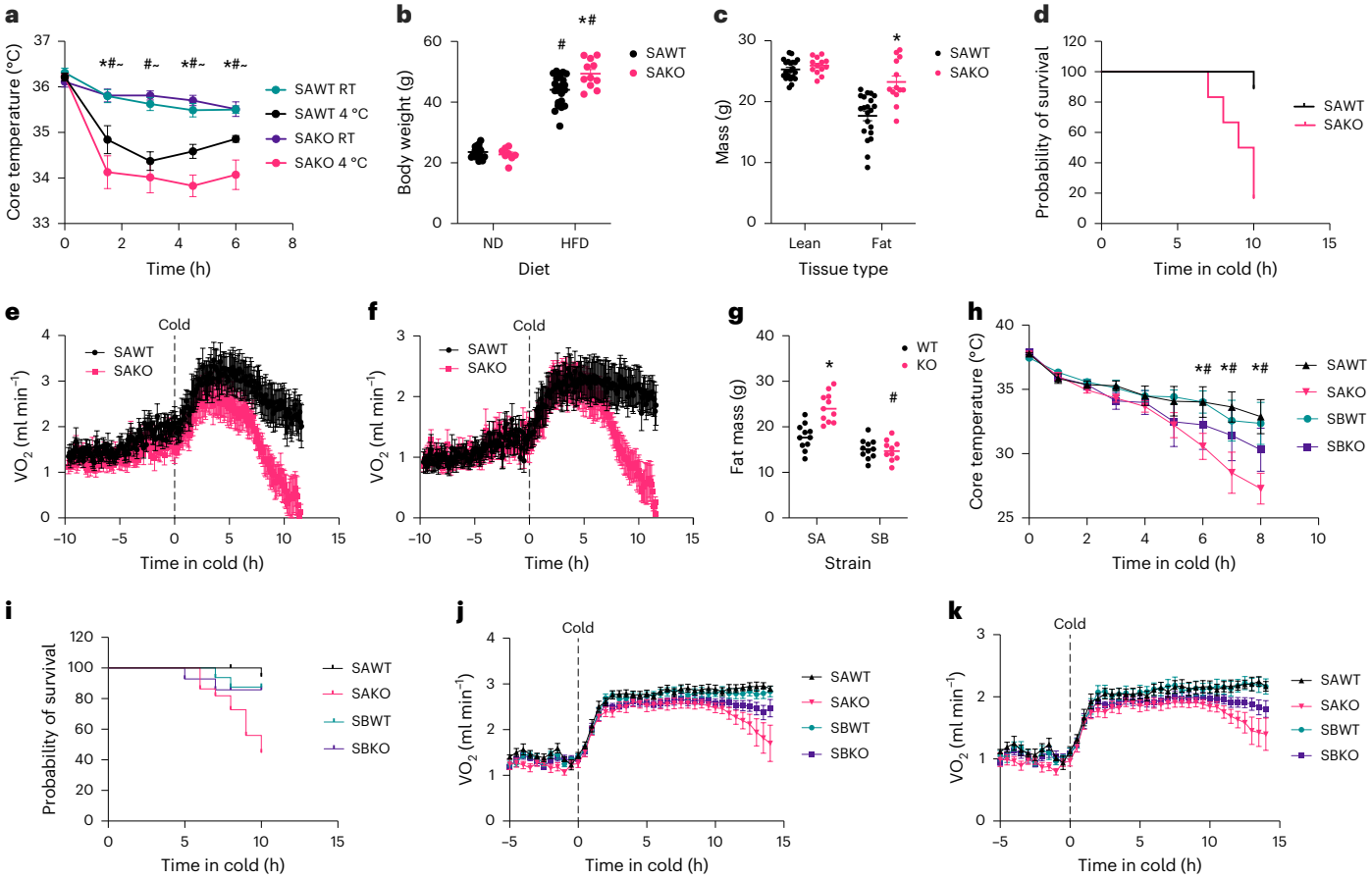

Fig. 5 | Obese thermoneutral-adapted SAKO mice exhibit a defect in cold tolerance. a, Core body temperature in obese male SAKO and SAWT mice during acute cold exposure at 4 °C or room temperature (RT), $n = 8$ mice except SAWT RT $n = 7$ mice; $^{*}P < 0.05$ SAWT 4 °C versus SAKO 4 °C; $^{\#}P < 0.05$ SAWT RT versus SAWT 4 °C; $^{\sim}P < 0.05$ SAKO RT versus SAKO 4 °C. **b**, Body weight in male SAWT and SAKO mice fed normal diet (ND) or HFD, $n = 16$ ND SAWT, 23 HFD SAWT, 8 ND SAKO and 11 HFD SAKO mice; $^{*}P = 0.001$ SAWT versus SAKO; $^{\#}P < 0.0001$ ND versus HFD. **c**, Lean and fat mass in obese male SAWT and SAKO mice housed at thermoneutrality (30 °C) for 3.5 months, $n = 21$ SAWT and 13 SAKO mice; $^{*}P < 0.0001$ SAWT versus SAKO. **d**–**f**, Survival (**d**), oxygen consumption (VO_2; **e**) and carbon dioxide production (VCO_2; **f**) in obese male SAWT and SAKO mice housed at 30 °C for 1 month and exposed to cold at 5 °C, $n = 9$ SAWT and 6 SAKO mice; SAWT versus SAKO $P = 0.003$ for survival and $P < 0.05$ at multiple time points after 10 h for VO_2 and VCO_2. **g**, Fat mass in obese male SAWT/KO and SBWT/KO mice housed at 30 °C for 3 months, $n = 11$ mice per group except SBKO $n = 10$ mice; $^{*}P < 0.05$ WT versus KO; $^{\#}P < 0.05$ SA versus SB. **h**, Core body temperature during acute cold exposure in obese thermoneutral-adapted male SAWT/KO and SBWT/KO mice, $n = 6$ mice per group; $^{*}P < 0.05$ SAWT versus SAKO. **i**, Survival during cold exposure in obese thermoneutral-adapted male SAWT/KO and SBWT/KO mice, $n = 21$ SAWT, 20 SAKO, 16 SBWT and 14 SBKO mice; $P = 0.85$ SBKO versus SBWT and $P = 0.0004$ SAKO versus SAWT. **j**,**k**, VO_2 (**j**) and VCO_2 (**k**) in obese thermoneutral-adapted male SAWT/KO and SBWT/KO mice maintained at 30 °C and transitioned to cold at time zero, $n = 10$ KO, 9 SAWT and 13 SBWT mice; $P < 0.05$ SAWT versus SAKO from 11 h; SAKO versus SBKO from 12.5 h (**j**) and 13 h (**k**); SBWT versus SBKO from 13.5 h (**k**). Data are mean ± s.e.m. Statistical significance was determined by two-way ANOVA with Holm–Šidák correction (**a**–**c**,**e**–**h**,**j**,**k**) or Gehan–Breslow–Wilcoxon test (**d**,**i**); exact P values are provided in the Source Data[68].

before levelling off at 32–33 °C (Fig. 6a). Core body temperature and energy expenditure dropped equally in SAWT and SAKO mice upon immobilization (Fig. 6a,b). Injection of CL-316,243 after immobilization protected core body temperature in obese thermoneutral-adapted control mice (Fig. 6c). While core body temperature was significantly higher in SAWT CL-316,243-injected mice as compared with vehicle controls, CL-316,243 did not significantly increase core temperature in the SAKO mice, whose temperature was significantly lower than that of the SAWT CL-316,243-treated mice (Fig. 6c). Importantly, the lipolytic response to CL-316,243 in the SAKO mice was not defective; serum fatty acid levels were increased equally in the SAWT and SAKO mice treated with CL-316,243 (Fig. 6d). Consistent with normal cold tolerance, SBKO mice did not exhibit a defect in lipolysis-driven thermogenesis (Fig. 6e), indicating that lipolysis-driven thermogenesis requires STAT3 in white adipocytes, while brown adipocyte STAT3 expression is dispensable. Female SAKO and SAWT mice were placed on an HFD for 30 weeks to achieve weight gain comparable to males (Fig. 6f). A defect in CL-316,243-induced thermogenesis was also observed in female SAKO mice relative to SAWT controls (Fig. 6g). The thermogenic defect in both male and female SAKO mice was corrected by pretreatment with the DGAT1 inhibitor PF-04620110 (Fig. 6h,i), consistent with STAT3-mediated repression of esterification as the mechanism of induction of oxidative metabolism and thermogenesis. DGAT inhibition did not impact fatty acid levels in the serum (Fig. 6j).

Fatty acids released by lipolytic white adipocytes fuel oxidative metabolism in other tissues. To determine the impact of fatty acid oxidation in vivo, we utilized etomoxir pretreatment in obese thermoneutral-adapted mice immobilized with pentobarbital. Etomoxir did not impact serum fatty acid levels at baseline or after lipolytic stimulation (Fig. 6k). No suppression of lipolysis-driven thermogenesis was observed with etomoxir pretreatment; in fact, thermogenesis was enhanced at early time points (Fig. 6l). This result indicates that thermoneutral housing and pentobarbital immobilization limited β-oxidation in brown fat and muscle and that thermogenesis in this context is independent of fatty acid oxidation.

A thermal probe was implanted into a cohort of SAWT and SAKO mice to obtain simultaneous core temperature and energy expenditure readings. After pentobarbital injection, core temperature and

https://doi.org/10.1038/s42255-026-01467-2

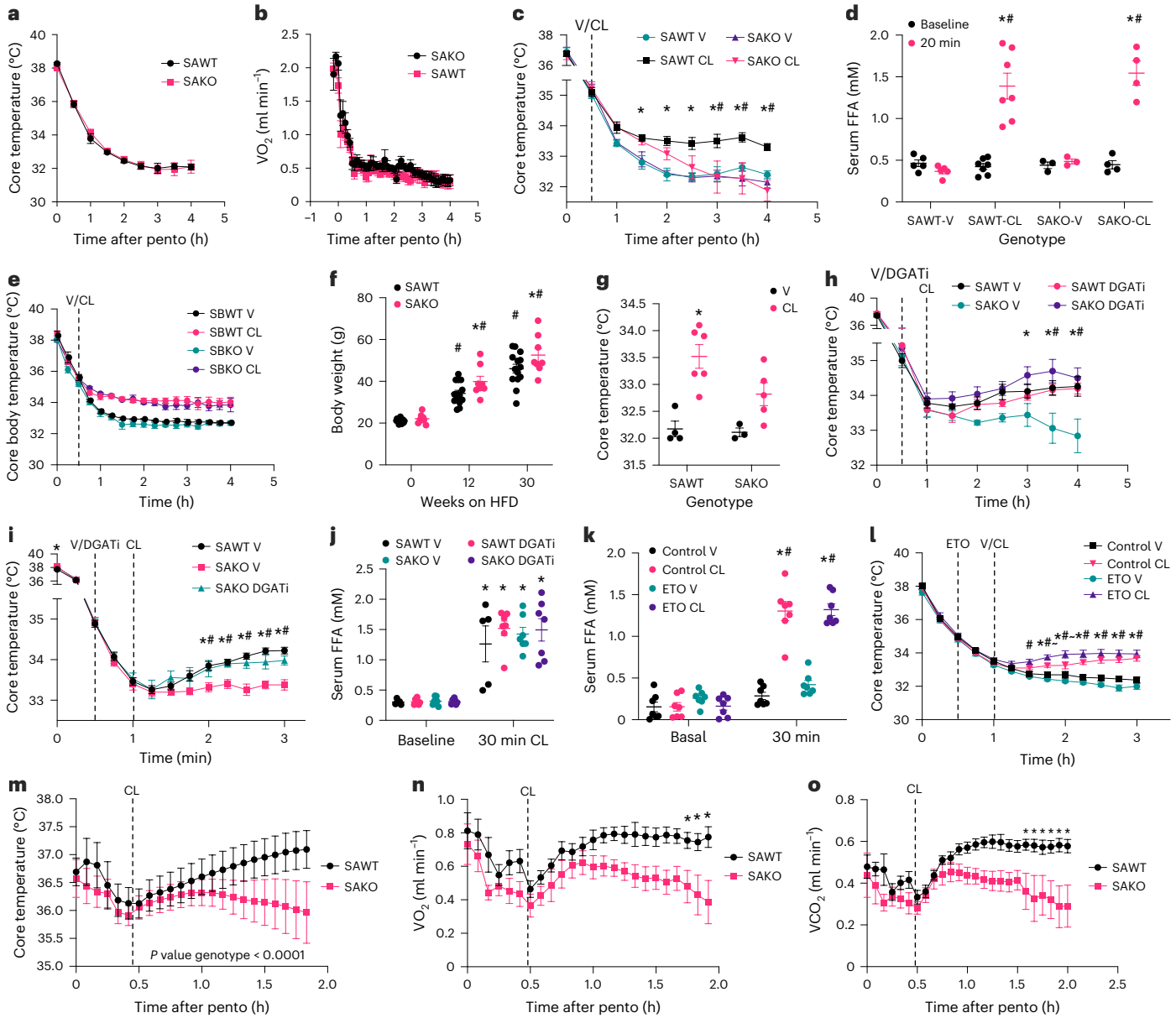

Fig. 6 | Lipolysis-driven thermogenesis is independent of physical activity. **a**,**b**, Core body temperature (**a**) and oxygen consumption (VO_2; **b**) in obese thermoneutral male SAWT and SAKO mice housed at 30 °C for 2 months and injected with pentobarbital (pento) at time zero to block muscle activity, $n = 8$ mice. **c**, Core body temperature in obese thermoneutral male SAWT and SAKO mice housed at 30 °C for 1 month and injected with pentobarbital at time zero followed by 1 mg kg^{-1} CL or V at 30 min, $n = 5$ mice except SAKO V $n = 4$ mice; *$P < 0.05$ SAWT V versus SAWT CL; $^{\#}P < 0.05$ SAWT CL versus SAKO CL. **d**, Serum FFA levels at baseline and 20 min after V or CL injection in obese thermoneutral male SAWT and SAKO mice housed at 30 °C for 2 months, $n = 5$ SAWT V, 7 SAWT CL, 3 SAKO V and 4 SAKO CL mice; *$P < 0.0001$ baseline versus 20 min; $^{\#}P < 0.0001$ V versus CL. **e**, Core body temperature in obese thermoneutral-adapted male SBWT and SBKO mice injected with pentobarbital at time zero followed by 1 mg kg^{-1} CL or V at 30 min, $n = 3$ SBWT V and SBKO CL mice and $n = 4$ SBWT CL and SBKO V mice; $P < 0.01$ V versus CL from 1 h. **f**, Body weight of female SAWT and SAKO mice fed HFD, $n = 14$ SAWT and 8 SAKO mice; *$P < 0.05$ SAWT versus SAKO; $^{\#}P < 0.0001$ versus younger age. **g**, Core body temperature in obese thermoneutral female SAWT and SAKO mice housed at 30 °C for 2 months and injected with pentobarbital 2 h after administration of 1 mg kg^{-1} CL or V, $n = 4$ SAWT V, 3 SAKO V, 6 SAWT CL and 5 SAKO CL mice; *$P = 0.0017$ SAWT V versus SAWT CL. **h**,**i**, Core body temperature in obese thermoneutral male (**h**) and female (**i**) mice injected with pentobarbital at time zero followed by 3 mg kg^{-1} DGATi or V at 30 min, with all mice receiving 1 mg kg^{-1} CL at 60 min, $n = 5$ male mice and $n = 8$ SAWT and 5 SAKO female mice; *$P < 0.05$ SAKO V versus SAKO DGATi; $^{\#}P < 0.05$ SAWT V versus SAKO V. **j**, Serum FFA levels at baseline and 30 min after V or CL injection, $n = 5$ SAWT and 7 SAKO mice. **k**, Serum FFA levels at baseline and 30 min after V or CL injection, $n = 7$ mice. In **j** and **k**, *$P < 0.0001$ baseline versus 30 min; $^{\#}P < 0.0001$ V versus CL. **l**, Core body temperature in obese thermoneutral female mice housed at 30 °C for over 6 months and injected with pentobarbital at time zero followed by 5 mg kg^{-1} ETO or V at 30 min and V or 1 mg kg^{-1} CL at 60 min, $n = 7$ mice; *$P < 0.05$ V versus CL; $^{\#}P < 0.05$ ETO V versus ETO CL; $^{-}P < 0.05$ control CL versus ETO CL. **m**–**o**, Core body temperature (**m**), oxygen consumption (VO_2; **n**) and carbon dioxide production (VCO_2; **o**) in obese thermoneutral male SAWT and SAKO mice housed at 30 °C for 1 month with implanted temperature probes and injected with 1 mg kg^{-1} CL, $n = 6$ SAWT and 5 SAKO mice; *$P < 0.05$ SAWT versus SAKO. Data are mean ± s.e.m. Statistical significance was determined by two-way ANOVA with Holm–Šidák correction; exact P values are provided in the Source Data[68].

https://doi.org/10.1038/s42255-026-01467-2

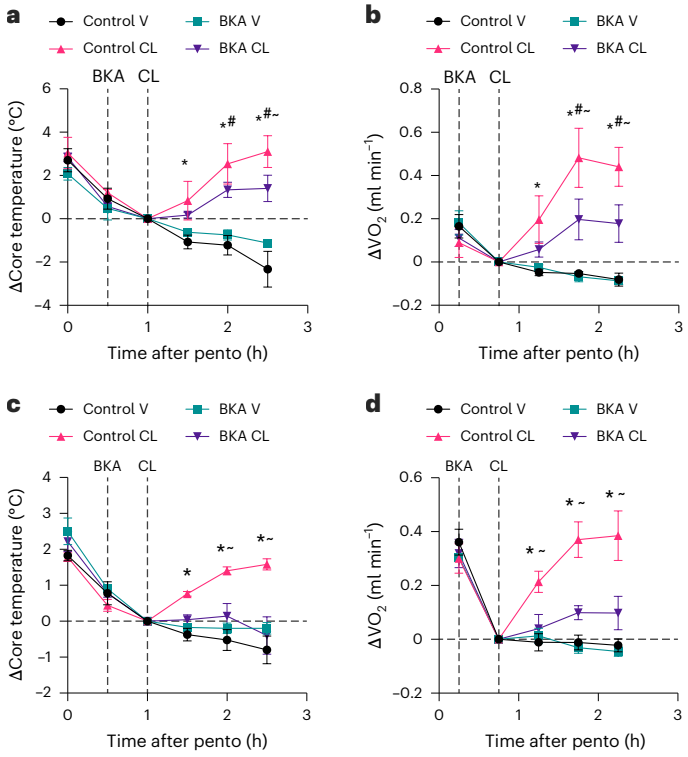

Fig. 7 | AAC-dependent thermogenesis. Male C57BL/6 mice were injected with pentobarbital at time zero and placed in metabolic cages at 30 °C. BKA 1 mg kg^{-1} or V was administered at 30 min, followed by CL 1 mg kg^{-1} or V at 60 min. **a**,**b**, Change in core body temperature (**a**) and oxygen consumption (VO_2; **b**) in male mice fed a normal diet and housed at room temperature, $n = 4$ V and 3 CL mice. **c**,**d**, Core body temperature (**c**) and oxygen consumption (**d**) in obese thermoneutral-adapted male mice, $n = 4$ V and 5 CL mice. **a**–**d**, $^{*}P < 0.05$ control V versus control CL; $^{\#}P < 0.05$ BKA V versus BKA CL; $^{\sim}P < 0.05$ control CL versus BKA CL. Data are mean ± s.e.m. Statistical significance was determined by two-way ANOVA with Holm–Šidák correction; exact *P* values are provided in the Source Data[68].

oxidative metabolism were reduced similarly in SAWT and SAKO mice (Fig. 6m–o). However, the two genotypes diverged upon CL-316,243 injection, which resulted in significantly higher core body temperature, oxygen consumption and carbon dioxide production in the SAWT compared with the SAKO mice (Fig. 6m–o). These data suggest that the thermogenic effect of CL-316,243 in obese thermoneutral-adapted mice is dependent on adipocyte STAT3 but independent of muscle activity, consistent with a thermogenic effect of lipolysis-driven oxidative metabolism in white adipocytes.

UCP1-dependent versus AAC-dependent thermogenesis

Our results suggest that fatty acid-driven uncoupling and thermogenesis is a universal property of adipocytes, and not limited to brown adipocytes. We propose that in white adipocytes fatty acid uncoupling is mediated by AAC, while in brown adipocytes UCP1 evolved to perform this function more effectively. UCP1-mediated uncoupling is the only AAC-independent thermogenic pathway as AAC is required for ATP-dependent futile cycles and shivering in addition to uncoupling. To dissect UCP1-mediated thermogenesis from AAC-dependent thermogenic pathways we investigated the impact of BKA in vivo. In normal-diet, room temperature-housed mice, lipolysis-induced thermogenesis was insensitive to BKA pretreatment, consistent with UCP1-mediated uncoupling in brown adipose tissue (Fig. 7a,b). However, pretreatment with BKA attenuated the increase in core body temperature and respiration in response to lipolytic activation in obese thermoneutral-adapted mice (Fig. 7c,d). Together, these data indicate that while lean mice rely primarily upon UCP1-mediated uncoupling for non-shivering thermogenesis, obese thermoneutral-adapted mice utilize AAC-dependent pathways (Extended Data Fig. 10).

Discussion

Adipocytes have three critical metabolic functions: energy storage, energy mobilization and thermogenesis. White adipocytes have tremendous storage capacity, while brown adipocytes specialize in thermogenesis. Still, brown adipocytes are capable of storage and white adipocytes are capable of thermogenesis. Beige adipocytes are observed in the inguinal adipose tissue of mice, after cold adaptation. Similar to brown adipocytes, beige adipocytes express UCP1 which, in conjunction with mitochondrial biogenesis, dramatically increases thermogenic capacity. The data presented here suggest that respiration in white adipocytes is uncoupled by fatty acids in complex with AACs, rather than UCP1. This thermogenic mechanism is distinct from ATP-dependent futile cycles that have been demonstrated to contribute to thermogenesis in brown and beige adipocytes[61–63].

It is well documented that cultured white adipocytes exhibit uncoupled respiration upon lipolytic stimulation[6,9,11–14,18]. Additionally, AACs have been proven to uncouple in the presence of fatty acids[16,17,38–47]. However, the molecular mechanism of white adipocyte uncoupling has not been elucidated. We used the AAC-specific inhibitor BKA as well as AAC2 knockdown in cultured adipocytes to interrogate this mechanism. The results consistently support AAC-mediated uncoupling in lipolytic white adipocytes. This mechanism is further supported by in vivo studies in obese thermoneutral-adapted C57Bl/6 mice. Together, these studies establish AAC-mediated uncoupling in lipolytic white adipocytes as a physiologically relevant thermogenic pathway.

While AAC-mediated uncoupling in the presence of fatty acids was first postulated in the 1960s, a lack of in vivo empirical evidence has called into question its physiological importance. Previous studies have demonstrated that fatty acids promote uncoupled respiration in isolated muscle mitochondria from animals such as fur seals, hibernating ground squirrels, rats and mice[39,64–66]. A 1984 publication reported that perfusion of rat livers with physiological levels of free fatty acids resulted in uncoupled respiration and an increase in oxygen consumption that could not be accounted for by fatty acid oxidation; in fact fatty acid oxidation was shown to be dispensable for the induction of respiration by fatty acids[67]. Consistent with these studies, we observed that mitochondrial import of fatty acyl-CoA via the carnitine shuttle was not required for lipolysis-driven uncoupled respiration. This result indicates that mitochondrial β-oxidation is dispensable, suggesting that other substrates such as glucose can be utilized. The dispensability of fatty acyl-CoA import supports free fatty acid interaction with AAC as the mechanism of uncoupling. Fatty acids can flip-flop though membranes in the protonated state, and there is evidence that the pK_a of fatty acids in the membrane is significantly lower than their pK_a in aqueous solution, facilitating phosphorylation on the membrane and movement into the mitochondrial inner membrane where they interact with AAC to promote uncoupling[65]. Notably, long-chain fatty acyl-CoA synthetases are absent from the mitochondrial matrix, prohibiting β-oxidation of free fatty acids in the mitochondrial inner membrane.

Non-shivering thermogenesis in lean standard-housed mice was observed to be AAC-independent, consistent with UCP1-mediated thermogenesis in brown adipose tissue[55–59]. Conversely, in obese thermoneutral-housed mice, thermogenesis was AAC-dependent, consistent with AAC-mediated uncoupling in white adipocytes—or coupled respiration. To specifically investigate the role of lipolysis-driven uncoupled respiration in white adipocytes, we utilized adipocyte-specific STAT3 KO mice, which display a defect in white adipocyte uncoupling without impacting the rate of lipolysis. In addition to the previously reported sensitivity to diet-induced obesity, adipocyte-specific STAT3 KO mice fed an HFD and housed at thermoneutrality exhibit cold intolerance relative to floxed littermate controls.

The white fat-specific defect in lipolysis-driven thermogenesis in these mice was reversed by pretreatment with PF-04620110, an orally bioavailable inhibitor of DGAT1[23]. This result ties the cold sensitivity phenotype specifically to fatty acid deposition in white adipocytes.

The absence of a phenotype in lean adipocyte-specific STAT3 KO mice argues against confounding effects in brown fat, supporting white adipocyte specificity of this thermogenic pathway. In lean animals, under standard housing conditions, thermogenic demands are high, activating brown adipocyte thermogenesis. Together, these studies, along with previous metabolic phenotyping, reduce concerns about confounding effects of adipocyte-specific STAT3 KO on other metabolic pathways[6]. A limitation of the study is the lack of an in vivo genetic model targeting adipocyte AAC expression. Consistent with our model, adipocyte-specific KO of *Slc25a5* has been reported to reduce adipocyte oxygen consumption and increase adipocyte size and adiposity[45]. However, the metabolic and thermogenic response to catecholamine stimulation has not been studied in these animals. These earlier studies suggest that a potential pitfall of increasing adipocyte respiration could be induction of hypoxia[44,45].

There is great interest in targeting adipocyte thermogenesis to increase energy expenditure and promote weight loss. However, classic thermogenic brown and beige adipocytes are scarce in adults, particularly in individuals with obesity[64–66]. In contrast, white adipocytes are hyperplastic in obesity. Despite their lower respiratory capacity per cell, the sheer abundance of white adipocytes makes them a compelling target for enhancing whole-body energy expenditure. Uncoupling in white adipocytes could represent a new target for obesity treatment. Given the overabundance of white adipose tissue in obesity, even a small increase in energy expenditure could have a substantial impact on whole-body energy balance. This treatment strategy would be complementary to current incretin-mimetic therapies, which reduce food intake[67].

One challenge in targeting AAC-mediated uncoupling is the requirement for AAC activity during coupled respiration, which is dependent on nucleotide exchange by the AACs. To date, these two functions have not been separated. AAC mutants that have been demonstrated to be defective in uncoupling activity also exhibit defects in nucleotide transport[17,38,46,47]. The relative uncoupling versus nucleotide transport capacity of AAC isoforms is unknown but could hold clues to these two functions. In murine adipocytes AAC2 is the dominant isoform. In human adipocytes, AAC3 expression is highest[9]. Interestingly, AAC2 is X-linked and AAC3 is pseudo autosomal. In vivo studies were primarily performed in male mice. However, the phenotype was also observed in obese female SAKO mice. No impact of cellular sex was observed in cultured adipocytes, and female donors were frequently used for efficiency.

Adipocyte fatty acid handling is of fundamental importance to adipocyte biology. Lipolysis floods adipocytes with fatty acids, changing adipocyte metabolism and whole-body energy balance. We previously reported that fatty acids stimulate serine 727 phosphorylation of STAT3, promoting its interaction with and repression of GPAT3 at the lipid droplet[6]. The current studies indicate AAC-mediated mitochondrial uncoupling in white adipocytes when fatty acid levels are elevated. As a result, lipolysis drives uncoupled respiration in white adipocytes, impacting whole-body energy expenditure and thermogenesis. We hope these findings will lay the groundwork for future studies investigating fatty acid handling in adipocytes and its impact on energy balance and metabolic health in additional animal models and human adipocytes.

Methods

Ethical compliance

All research described in this study was conducted in accordance with relevant institutional and national ethical guidelines and regulations. All animal experiments were approved by the Institutional Animal Care and Use Committee at Weill Cornell Medicine and performed in compliance with institutional and federal regulations governing the humane treatment of research animals.

Reagents

The following reagents were used in this study: amphotericin B (Sigma catalogue number A2411), antimycin A (Sigma catalogue number A8674), atglistatin (Sigma catalogue number SML1075), BKA (Enzo catalogue number BML-CM113), carbonyl cyanide 4-(trifluoromethoxy) phenylhydrazone (FCCP, Sigma catalogue number C2920), CL-316,243 (Sigma catalogue number C5979), collagenase (Sigma catalogue number C6885), CSA (Enzo catalogue number BML-A195), dexamethasone (Sigma catalogue number D4902), DMEM/F-12 50/50 (Corning catalogue number 15-090), etomoxir (AmBeed catalogue number A108121), fetal bovine serum (FBS, Corning catalogue number 35-010), extracellular matrix gel from Engelbreth–Holm–Swarm murine sarcoma (Sigma catalogue number E1270), fibronectin (Sigma catalogue number F1141) forskolin (Sigma catalogue number F3917), FS high-glucose DMEM (Cytiva SH30243), hexadimethrine bromide (polybrene) (Sigma catalogue number H9268), insulin (Sigma catalogue number I6634), 3-isobutyl-1-methylxanthine (Sigma catalogue number I5879), isoproterenol (Sigma catalogue number PHR2722), JC-10 (AAT Bioquest catalogue number 22204), Lenti-X Packaging Single Shots (Takara catalogue number 631276), Maxiprep Kit (Qiagen catalogue number 12162), Miniprep Kit (Qiagen catalogue number 27106), MitoTracker Green (Fisher catalogue number M7514), norepinephrine (Sigma catalogue number A7257), Oligomycin A (Sigma catalogue number 75351), Pen Strep Glutamine (Gibco catalogue number 10378-016), pentobarbital (Covetrus catalogue number 081799), PF-04620110 (DGATi, Sigma catalogue number PZ0207), pLKO.1 Backbone (Addgene Plasmid catalogue number 10879), poly lysine (Sigma catalogue number P1274), Puradisc sterile PES syringe filters (Cytiva catalogue number 6780-1304), puromycin (Sigma catalogue number P8833), rosiglitazone (Sigma catalogue number 557366), rotenone (Sigma catalogue number R8875), Stbl3 Competent *E. Coli* (Thermo Fisher catalogue number C737303), Tet approved FBS (Takara catalogue number 631107), TMRM (Fisher catalogue number I34361).

Animals

Animals homozygous for the *Stat3* floxed allele (Stock Number 016923) were bred to *Adipoq*-promoter-driven *Cre* mice (Stock Number 028020) to generate mice homozygous for the *Stat3* floxed allele both with and without the *Adipoq-Cre*. Animals with *Adipoq-Cre* expression lose *Stat3* in mature adipocytes and are referred to in the paper as SAKO animals, while floxed littermate controls without *Adipoq-Cre* are referred to as SAWT. Animals homozygous for the *Stat3* floxed allele were also bred to *Ucp1*-promoter-driven *Cre* mice (Stock Number 024670) to generate mice homozygous for the *Stat3* floxed allele both with and without the *Ucp1-Cre*. Animals with *Ucp1-Cre* expression model where the *Stat3* gene has been specifically lost in brown adipocytes and are referred to in the paper as SBKO animals, while floxed littermate controls without *Ucp1-Cre* are referred to as SBWT.

All strains of mice were on the C57BL/6J background (Stock Number 000664). Animals for experiments were bred in-house. Within an experiment, the genotype and/or treatment groups were littermates and/or cage mates. Mice were assigned to treatment groups, such that before treatment the mean body weight, as well as the standard deviation of the body weight, was equal across treatment groups, using a method similar to block randomization. Additional consideration was given to housing, such that each cage contained multiple treatment groups, to avoid confounding by cage effects. Animals in each cohort were produced from multiple breeding pairs to minimize the birthdate range. Extra attention was paid to housing arrangements to ensure that each cage accommodated multiple treatment groups, to minimize potential confounding by the cage effect. Treatment groups

were assigned during animal studies, and ear tag numbers were used to identify animals. Researchers performing tests and collecting data were blinded during experiments. Sample sizes were determined using a power analysis with the expected effect size but were sometimes limited by availability. Sex as a biological variable was considered; female and male cohorts were analysed separately.

Mice were housed in a specific-pathogen-free facility with a 12-h light/dark cycle and were given free access to food and water. Mice were fed normal diet (Labdiet, Picolab catalogue number 5053) or HFD (Research Diets catalogue number D12451) with 45% of calories from fat. Starting dates on the HFD were determined according to sex. Female groups were started on the HFD at 10–14 weeks of age, and males at 6–10 weeks of age. Thermoneutral-adapted mice were housed at 30 °C for a minimum of 1 month.

Body composition analysis. Body composition was determined at the Weill Cornell Medicine Metabolic Phenotyping Center using an EchoMRI (3 in 1) nuclear magnetic resonance analyser.

Indirect calorimetry (metabolic cage experiments). Mice were housed in Sable Systems International Promethion metabolic cages to measure oxygen consumption (VO_2), carbon dioxide production (VCO_2) via indirect calorimetry and spontaneous motor activity at the Weill Cornell Metabolic Phenotyping Center. Cages were situated in environmentally controlled chambers (catalogue number DB034-LT) for precise temperature control.

Acute cold exposure (5 °C) was performed in a climate-controlled room or environmental chamber. Mice were single-housed in standard housing cages or metabolic cages. Rectal temperature measurements were taken using a mouse rectal probe and thermometer (PhysiTemp catalogue number BAT-12).

Thermogenesis in immobilized mice. Mice were anaesthetized with an intraperitoneal injection of 70 mg kg^{-1} pentobarbital. Mice were intraperitoneally injected with up to 1 mg kg^{-1} CL-316,243 or PBS vehicle after 30 min. In experiments with intraperitoneally injected inhibitor pretreatment at 30 min (3 mg kg^{-1} DGATi, 5 mg kg^{-1} etomoxir, 1 mg kg^{-1} BKA or vehicle control), 1 mg kg^{-1} CL-316,243 treatment was administered at 60 min. The depth of anaesthesia was assessed every 15 to 30 min by applying noxious stimuli (for example, the pedal withdrawal reflex in the hind limbs). If any response was observed, 20 to 30 mg kg^{-1} pentobarbital was administered.

Temperature probe implantation. A G2 E-mitter temperature probe (Starr Life Sciences) was implanted in the peritoneal cavity of 6-week-old mice. Mice were anaesthetized with ketamine/xylazine and sterile lubricant applied to both eyes. The abdomen was shaved, and the surgical site sterilized. A 2-cm midline ventral incision was made 1 cm below the diaphragm. The skin was then retracted, and the abdominal cavity was opened by making a 1-cm incision along the posterior left lower quadrant. The temperature probe was positioned in the abdominal cavity ventral to the digestive organs. Local anaesthetic was applied, and the abdominal cavity was closed using monofilament absorbable sutures and wound clips. Post-surgical pain was managed with buprenorphine and meloxicam. At 2 weeks after the operation, mice were placed on HFD then thermoneutral-adapted for the experiment.

In vivo lipolysis. Blood was collected by submandibular bleed, coagulated and centrifuged at 10,000*g* for 10 min at 4 °C to separate the serum. For free fatty acid measurement, 2 µl of serum was used with the NEFA Linearity Set (Wako's NEFA HR 2, 999-34691- 991-34891- 995-34791- 993-35191). The assay was performed using 75 µl of Reagent A and 150 µl of Reagent B. Absorbance was measured at 550 nm with a reference wavelength of 660 nm, following the manufacturer's protocol.

Real-time PCR analysis of gene expression. Adipose tissue was homogenized in Trizol (Invitrogen) and mixed with 20% chloroform. RNA extractions from inguinal white adipose tissue, epididymal white adipose tissue and brown adipose tissue were performed using the PureLink RNA Mini Kit (Thermo Fisher Scientific catalogue number 12183020). We used SuperScript IV VILO Master Mix Synthesis System for reverse-transcription PCR (Thermo Fisher Scientific catalogue number 11766050) with a 3:1 mixture of random hexamers to oligo dT primers for reverse transcription. Real-time PCR amplification was performed on samples in triplicate with Power SYBR Green PCR Master Mix (Applied Biosystems catalogue number A46109) using the Applied Biosystems QuantStudio5 real-time PCR System and quantified using an internal standard curve with *Arbp* as the control gene. Primer sequences were obtained from the Harvard primer bank or generated using Primer3. Primer specificity was validated using NCBI primer-BLAST. Primer sequences are listed in Supplementary Table 1.

Cell culture

Lentivirus production. Knockdown target sequences were generated by inputting the NCBI gene ID into Broad Institute's Genetic Perturbation Platform online tool, and oligo sequences cloned into the pLKO.1 digested with EcoRI-HF and AgeI-HF are listed in Supplementary Table 2. Lenti-X 293T (Takara catalogue number 632180) cells were seeded in 10-cm culture plates to reach 70–80% confluence by the time of transfection the next morning. Medium was removed and replaced with 5 ml of high-glucose DMEM with 10% Tet system-approved FBS and no antibiotics. Lenti-X Packaging Single Shots were mixed with 7 µg of pLKO.1 plasmids and added drop-wise to Lenti-X 293T plates. After at least 4 h, another 6 ml of medium was added to each plate. At 48–72 h post transfection, all medium was removed from 293T plates and centrifuged (500*g* for 10 min). The supernatant was filtered through a 0.45-µm polyethersulfone syringe filter. Before use, 10 µg ml^{-1} hexadimethrine bromide and insulin were added to the viral supernatant media.

Primary adipocytes. Primary preadipocytes were isolated from inguinal fat pads as follows: Following fine mincing, the tissue was digested with 1 mg ml^{-1} collagenase and 2% BSA in a 37 °C water bath with shaking for 20–35 min. The digestion was stopped by adding 15% FBS media 1:1 to the serum-free collagenase media, then the slurry was passed through a 100-µm filter and spun at 500*g* for 5 min. The pellet was washed and resuspended in culture media (DMEM/F-12 with 15% FBS and Pen Strep Glutamine) and plated with 2.5 mg l^{-1} amphotericin B and placed in a 10% CO_2 incubator. Non-adherent cells were washed away 3 d later. When the cells reached ~80% confluence, they were passaged from their original 10-cm culture plate to a 15-cm plate and incubated for an additional 2–5 d. Cells from the second passage were plated to confluence for experiments on extracellular matrix and fibronectin-coated plates. Differentiation was initiated with 500 µM 3-isobutyl-1-methylxanthine, 5 µM dexamethasone, 1 µg ml^{-1} insulin and 1 µM rosiglitazone for 3 d, followed by insulin alone for at least 3 d. For knockdown experiments, viral transduction was performed after the third day in differentiation media. After 16–18 h of incubation, medium was replaced with adipocyte medium containing insulin only. The following day, 2 µg ml^{-1} puromycin was added to the medium to select for transduced cells. In all experiments, medium was replaced every 2 d until experiments were conducted 5–7 d after transduction. Cells were used for experiments 7–10 d after the initiation of differentiation. At 24 h before the start of an assay, insulin was removed from the culture media. Only cultures in which over 90% of cells displayed adipocyte morphology were used. Wells in which the adipocytes had become detached, or differentiation rates were under 90%, were identified visually and omitted.

3T3-L1 adipocytes. 3T3-L1 fibroblasts (obtained from the Saltiel lab) were differentiated as previously described[49].

Seahorse respiration assays. Extracellular oxygen consumption rates were measured with a Seahorse XFe96 analyser. Primary preadipocytes were differentiated in 96-well Seahorse XFe96 culture plates. After differentiation, cells were switched to Seahorse XF base DMEM (Agilent catalogue number 102353) supplemented with 2 mM glutamine, 1 mM pyruvate and 8 mM glucose. Pre-treatments were added to the base medium. During the assays, drug treatments were injected sequentially using the ports. Unless otherwise indicated, Port A contained 100 nM CL-316,243 or vehicle control; Port B: 2 µM oligomycin; Port C: 1 µM FCCP; and Port D: 1 µM rotenone and 1 µM antimycin A.

Mitochondrial membrane potential. TMRM staining was performed and imaged with an imageXpress MICRO Confocal Automated High-Content Analysis System to visualize live mitochondrial membrane potential. Cells were stained with 200 nM TMRM for 30 min at 37 °C, then washed three times with PBS. Imaging was performed in live cell imaging solution (Invitrogen catalogue number A59688DJ). After baseline images were obtained, cells were treated with either vehicle control or CL-316,243. Finally, cells were treated with 1 µM FCCP as a negative control for membrane potential. Four technical replicates were imaged for each well and then averaged, and statistics were performed by well. For JC-10 membrane potential experiments, cells were incubated with JC-10 at 15 µM for 30 min at 37 °C, washed three times and changed to live cell imaging solution. Images were acquired using the same protocol as with TMRM but with both a TRITC and FITC channel image at each site, capturing the ratio of red to green fluorescence.

Western blot analysis. Subcellular fractionation was performed as previously described[6]. Briefly, cells were Dounce homogenized in fractionation buffer, and mitochondria were pelleted by a 10,000*g* spin of the supernatant from a 1,000 g. Proteins were resolved by SDS–PAGE and transferred to nitrocellulose membranes (Bio-Rad). Individual proteins were detected with specific primary antibodies and horseradish-peroxidase-conjugated secondary antibodies (Bio-Rad), then visualized with Western Lightning Enhanced Chemiluminescence (Perkin Elmer Life Sciences) using a ChemiDoc MP imaging system (Bio-Rad). Primary AAC2 (catalogue number 14671), H3 (catalogue number 4499), STAT3 (catalogue number 9139), TOM20 (catalogue number 42406) and UCP1 (catalogue number 72298) antibodies were purchased from Cell Signaling and used at a 1:1,000 dilution. AAC1 primary (1:1,000; catalogue number MA5-55372) and goat anti-mouse (1:10,000; catalogue number 31430) and goat anti-rabbit (1:10,000; catalogue number 31460) secondary antibodies were purchased from Thermo Fisher. Uncropped western blot scans with the size markers indicated are included in the Source Data. Replicate blots were run, transferred and blotted in parallel.

Lipolysis assay. Lipolysis in primary adipocytes was performed as previously decribed[50]; the linear rate was quantified from serial sampling of fatty acid and glycerol released into DMEM with 5% BSA, unless otherwise indicated.

Statistics and reproducibility

Two-way or one-way analysis of variance (ANOVA) was performed to evaluate statistical significance, followed by the Holm–Sidak post hoc analysis to determine specific between-group and time-dependent differences. For statistical comparison of only two groups, an *f*-test was performed first, and, if significant, a non-parametric two-tailed *t*-test employed. Survival rates were analysed using a Gehan–Breslow–Wilcoxon test. All *P* values were adjusted for multiple comparisons. In each case, significance was set at $\alpha < 0.05$, and data are presented as mean ± s.e.m. Statistical analyses were performed in GraphPad Prism version 10. The results presented have been replicated in at least three separate experiments, and data shown are representative of and consistent with other experiments.

Reporting summary

Further information on research design is available in the Nature Portfolio Reporting Summary linked to this article.

Data availability

The experimental data and statistical analyses that support the findings of this study are available via figshare at https://doi.org/10.6084/m9.figshare.27022276 (ref. 68). Source data are provided with this paper.

References

1. Ghaben, A. L. & Scherer, P. E. Adipogenesis and metabolic health. *Nat. Rev. Mol. Cell Biol.* **20**, 242–258 (2019).
2. Mann, J. P. & Savage, D. B. What lipodystrophies teach us about the metabolic syndrome. *J. Clin. Invest.* **129**, 4009–4021 (2019).
3. Angel, A., Desai, K. & Halperin, M. L. Free fatty acid and ATP levels in adipocytes during lipolysis. *Metabolism* **20**, 87–99 (1971).
4. Vaughan, M. The production and release of glycerol by adipose tissue incubated in vitro. *J. Biol. Chem.* **237**, 3354–3358 (1962).
5. Vaughan, M. & Steinberg, D. Effect of hormones on lipolysis and esterification of free fatty acids during incubation of adipose tissue in vitro. *J. Lipid Res.* **4**, 193–199 (1963).
6. Reilly, S. M. et al. Catecholamines suppress fatty acid re-esterification and increase oxidation in white adipocytes via STAT3. *Nat. Metab.* **2**, 620–634 (2020).
7. Saggerson, E. D., Sooranna, S. R., Bates, E. J. & Cheng, C. H. Rapid effects of hormones on enzymes of lipid metabolism. *Biochem. Soc. Trans.* **7**, 854–857 (1979).
8. Leibel, R. L., Hirsch, J., Berry, E. M. & Gruen, R. K. Alterations in adipocyte free fatty acid re-esterification associated with obesity and weight reduction in man. *Am. J. Clin. Nutr.* **42**, 198–206 (1985).
9. Yehuda-Shnaidman, E., Buehrer, B., Pi, J., Kumar, N. & Collins, S. Acute stimulation of white adipocyte respiration by PKA-induced lipolysis. *Diabetes* **59**, 2474–2483 (2010).
10. Davis, R. J. & Martin, B. R. The effect of β-adrenergic agonists on the membrane potential of fat-cell mitochondria in situ. *Biochem. J.* **206**, 611–618 (1982).
11. Hepp, D., Challoner, D. R. & Williams, R. H. Respiration in isolated fat cells and the effects of epinephrine. *J. Biol. Chem.* **243**, 2321–2327 (1968).
12. Vallano, M. L., Lee, M. Y. & Sonenberg, M. Hormones modulate adipocyte membrane potential ATP and lipolysis via free fatty acids. *Am. J. Physiol.* **245**, E266–E272 (1983).
13. Vallano, M. L. & Sonenberg, M. Triphenylmethylphosphonium cation distribution as a measure of hormone-induced alterations in white adipocyte membrane potential. *J. Membr. Biol.* **68**, 57–66 (1982).
14. Cheng, K., Groarke, J., Osotimehin, B., Haspel, H. C. & Sonenberg, M. Effects of insulin, catecholamines, and cyclic nucleotides on rat adipocyte membrane potential. *J. Biol. Chem.* **256**, 649–655 (1981).
15. Li, Y., Fromme, T., Schweizer, S., Schottl, T. & Klingenspor, M. Taking control over intracellular fatty acid levels is essential for the analysis of thermogenic function in cultured primary brown and brite/beige adipocytes. *EMBO Rep.* **15**, 1069–1076 (2014).
16. Bertholet, A. M. et al. Mitochondrial uncouplers induce proton leak by activating AAC and UCP1. *Nature* **606**, 180–187 (2022).
17. Bertholet, A. M. et al. H^+ transport is an integral function of the mitochondrial ADP/ATP carrier. *Nature* **571**, 515–520 (2019).
18. Ball, E. G. & Jungas, R. L. On the action of hormones which accelerate the rate of oxygen consumption and fatty acid release in rat adipose tissue in vitro. *Proc. Natl Acad. Sci. USA* **47**, 932–941 (1961).
19. Husted, A. S. et al. Autocrine negative feedback regulation of lipolysis through sensing of NEFAs by FFAR4/GPR120 in WAT. *Mol. Metab.* **42**, 101103 (2020).

20. Fain, J. N. & Shepherd, R. E. Free fatty acids as feedback regulators of adenylate cyclase and cyclic 3′:5′-AMP accumulation in rat fat cells. *J. Biol. Chem.* **250**, 6586–6592 (1975).
21. Burns, T. W., Langley, P. E., Terry, B. E. & Robinson, G. A. The role of free fatty acids in the regulation of lipolysis by human adipose tissue cells. *Metabolism* **27**, 1755–1762 (1978).
22. Kalderon, B. et al. Suppression of adipose lipolysis by long-chain fatty acid analogs. *J. Lipid Res.* **53**, 868–878 (2012).
23. Dow, R. L. et al. Discovery of PF-04620110, a potent, selective, and orally bioavailable inhibitor of DGAT-1. *ACS Med. Chem. Lett.* **2**, 407–412 (2011).
24. Chitraju, C. et al. Triglyceride synthesis by DGAT1 protects adipocytes from lipid-induced ER stress during lipolysis. *Cell Metab.* **26**, 407–418 (2017).
25. Sharma, A. K. et al. Basal re-esterification finetunes mitochondrial fatty acid utilization. *Mol. Metab.* **71**, 101701 (2023).
26. Fain, J. N., Loken, S. C. & Czech, M. P. Oligomycin effects on lipolysis and the oxidative metabolism of brown fat cells. *Biochim. Biophys. Acta* **197**, 40–48 (1970).
27. Locke, R. M., Rial, E. & Nicholls, D. G. The acute regulation of mitochondrial proton conductance in cells and mitochondria from the brown fat of cold-adapted and warm-adapted guinea pigs. *Eur. J. Biochem.* **129**, 381–387 (1982).
28. Heaton, G. M. & Nicholis, D. G. Hamster brown-adipose-tissue mitochondria. The role of fatty acids in the control of the proton conductance of the inner membrane. *Eur. J. Biochem.* **67**, 511–517 (1976).
29. Nicholls, D. G. Hamster brown-adipose-tissue mitochondria. Purine nucleotide control of the ion conductance of the inner membrane, the nature of the nucleotide binding site. *Eur. J. Biochem.* **62**, 223–228 (1976).
30. Bertholet, A. M. & Kirichok, Y. UCP1: a transporter for H^+ and fatty acid anions. *Biochimie* **134**, 28–34 (2017).
31. Halestrap, A. P. & Davidson, A. M. Inhibition of Ca^{2+}-induced large-amplitude swelling of liver and heart mitochondria by cyclosporin is probably caused by the inhibitor binding to mitochondrial-matrix peptidyl-prolyl *cis-trans* isomerase and preventing it interacting with the adenine nucleotide translocase. *Biochem. J.* **268**, 153–160 (1990).
32. Connern, C. P. & Halestrap, A. P. Purification and N-terminal sequencing of peptidyl-prolyl *cis-trans*-isomerase from rat liver mitochondrial matrix reveals the existence of a distinct mitochondrial cyclophilin. *Biochem. J.* **284**, 381–385 (1992).
33. Tanveer, A. et al. Involvement of cyclophilin D in the activation of a mitochondrial pore by Ca^{2+} and oxidant stress. *Eur. J. Biochem.* **238**, 166–172 (1996).
34. Crompton, M. The mitochondrial permeability transition pore and its role in cell death. *Biochem. J.* **341**, 233–249 (1999).
35. Halestrap, A. P. What is the mitochondrial permeability transition pore? *J. Mol. Cell. Cardiol.* **46**, 821–831 (2009).
36. Beutner, G., Alavian, K. N., Jonas, E. A. & Porter, G. A. Jr. The mitochondrial permeability transition pore and ATP synthase. *Handb. Exp. Pharmacol.* **240**, 21–46 (2017).
37. Crompton, M., Ellinger, H. & Costi, A. Inhibition by cyclosporin A of a Ca^{2+}-dependent pore in heart mitochondria activated by inorganic phosphate and oxidative stress. *Biochem. J.* **255**, 357–360 (1988).
38. Kreiter, J. et al. FA sliding as the mechanism for the ANT1-mediated fatty acid anion transport in lipid bilayers. *Int. J. Mol. Sci.* **24**, 13701 (2023).
39. Andreyev, A. et al. The ATP/ADP-antiporter is involved in the uncoupling effect of fatty acids on mitochondria. *Eur. J. Biochem.* **182**, 585–592 (1989).
40. Brustovetsky, N. & Klingenberg, M. The reconstituted ADP/ATP carrier can mediate H^+ transport by free fatty acids, which is further stimulated by mersalyl. *J. Biol. Chem.* **269**, 27329–27336 (1994).
41. Kreiter, J. et al. ANT1 activation and inhibition patterns support the fatty acid cycling mechanism for proton transport. *Int. J. Mol. Sci.* **22**, 2490 (2021).
42. Sparks, L. M. et al. ANT1-mediated fatty acid-induced uncoupling as a target for improving myocellular insulin sensitivity. *Diabetologia* **59**, 1030–1039 (2016).
43. Shabalina, I. G., Kramarova, T. V., Nedergaard, J. & Cannon, B. Carboxyatractyloside effects on brown-fat mitochondria imply that the adenine nucleotide translocator isoforms ANT1 and ANT2 may be responsible for basal and fatty-acid-induced uncoupling respectively. *Biochem. J.* **399**, 405–414 (2006).
44. Lee, Y. S. et al. Increased adipocyte O_2 consumption triggers HIF-1α, causing inflammation and insulin resistance in obesity. *Cell* **157**, 1339–1352 (2014).
45. Seo, J. B. et al. Knockdown of Ant2 reduces adipocyte hypoxia and improves insulin resistance in obesity. *Nat. Metab.* **1**, 86–97 (2019).
46. Pebay-Peyroula, E. et al. Structure of mitochondrial ADP/ATP carrier in complex with carboxyatractyloside. *Nature* **426**, 39–44 (2003).
47. Nury, H. et al. Structural basis for lipid-mediated interactions between mitochondrial ADP/ATP carrier monomers. *FEBS Lett.* **579**, 6031–6036 (2005).
48. Henderson, P. J. & Lardy, H. A. Bongkrekic acid. An inhibitor of the adenine nucleotide translocase of mitochondria. *J. Biol. Chem.* **245**, 1319–1326 (1970).
49. Rodic, N. et al. DNA methylation is required for silencing of ant4, an adenine nucleotide translocase selectively expressed in mouse embryonic stem cells and germ cells. *Stem Cells* **23**, 1314–1323 (2005).
50. Levy, S. E., Chen, Y. S., Graham, B. H. & Wallace, D. C. Expression and sequence analysis of the mouse adenine nucleotide translocase 1 and 2 genes. *Gene* **254**, 57–66 (2000).
51. Lunardi, J., Hurko, O., Engel, W. K. & Attardi, G. The multiple ADP/ATP translocase genes are differentially expressed during human muscle development. *J. Biol. Chem.* **267**, 15267–15270 (1992).
52. Shin, H. et al. Lipolysis in brown adipocytes is not essential for cold-induced thermogenesis in mice. *Cell Metab.* **26**, 764–777 (2017).
53. Haemmerle, G. et al. Defective lipolysis and altered energy metabolism in mice lacking adipose triglyceride lipase. *Science* **312**, 734–737 (2006).
54. Schreiber, R. et al. Cold-induced thermogenesis depends on ATGL-mediated lipolysis in cardiac muscle, but not brown adipose tissue. *Cell Metab.* **26**, 753–763 (2017).
55. Smith, R. E., Roberts, J. C. & Hittelman, K. J. Nonphosphorylating respiration of mitochondria from brown adipose tissue of rats. *Science* **154**, 653–654 (1966).
56. Cannon, B. & Nedergaard, J. Brown adipose tissue: function and physiological significance. *Physiol. Rev.* **84**, 277–359 (2004).
57. Enerback, S. et al. Mice lacking mitochondrial uncoupling protein are cold-sensitive but not obese. *Nature* **387**, 90–94 (1997).
58. Golozoubova, V. et al. Only UCP1 can mediate adaptive nonshivering thermogenesis in the cold. *FASEB J.* **15**, 2048–2050 (2001).
59. Nedergaard, J. et al. UCP1: the only protein able to mediate adaptive non-shivering thermogenesis and metabolic inefficiency. *Biochim. Biophys. Acta* **1504**, 82–106 (2001).
60. Sveidahl Johansen, O. et al. Lipolysis drives expression of the constitutively active receptor GPR3 to induce adipose thermogenesis. *Cell* **184**, 3502–3518 (2021).
61. Chouchani, E. T., Kazak, L. & Spiegelman, B. M. New advances in adaptive thermogenesis: UCP1 and beyond. *Cell Metab.* **29**, 27–37 (2019).
62. Granneman, J. G., Burnazi, M., Zhu, Z. & Schwamb, L. A. White adipose tissue contributes to UCP1-independent thermogenesis. *Am. J. Physiol. Endocrinol. Metab.* **285**, E1230–E1236 (2003).

63. Rahbani, J. F. et al. Parallel control of cold-triggered adipocyte thermogenesis by UCP1 and CKB. *Cell Metab.* **36**, 526–540 (2024).
64. Becher, T. et al. Brown adipose tissue is associated with cardiometabolic health. *Nat. Med.* **27**, 58–65 (2021).
65. Cronin, C. G. et al. Brown fat at PET/CT: correlation with patient characteristics. *Radiology* **263**, 836–842 (2012).
66. Steinberg, J. D., Vogel, W. & Vegt, E. Factors influencing brown fat activation in FDG PET/CT: a retrospective analysis of 15,000+ cases. *Br. J. Radiol.* **90**, 20170093 (2017).
67. Drucker, D. J. GLP-1 physiology informs the pharmacotherapy of obesity. *Mol. Metab.* **57**, 101351 (2022).
68. Maryam, A. et al. NATMETAB-A240912867-T. Dataset. *figshare* https://doi.org/10.6084/m9.figshare.27022276 (2025).

Acknowledgements

This work was supported by the US National Institutes of Health grant no. R01DK126944 and Nachman Research Scholars award to S.M.R. We thank I. D. Gülkan and M. Kulaprathazhe for their assistance with genotyping, and P. Bridge-Comer for maintenance of animal colonies. 3T3-L1 fibroblasts were generously provided by A. R. Saltiel, and lentiviral pLKO.1 cloning plasmid and methodology kindly shared by P. Cohen.

Author contributions

M.A. was responsible for conceptualization, methodology and investigations. A.M.A. and Z.J.Z. were responsible for investigations, formal analysis, visualization, and reviewing and editing the paper. P.D. was responsible for methodology, investigations, formal analysis and visualization. M.A., A.M.A., P.D. and Z.J.Z. all contributed equally to this paper. Y.K., O.G. and S.J.C. performed investigations, formal analysis and visualization. N.G.-B. was responsible for resources, investigations and methodology. S.M.R. was responsible for conceptualization, methodology, investigations, formal analysis, visualization, writing the original draft, reviewing and editing the paper, supervision, and funding acquisition.

Competing interests

The authors declare no competing interests.

Additional information

Extended data is available for this paper at https://doi.org/10.1038/s42255-026-01467-2.

Supplementary information The online version contains supplementary material available at https://doi.org/10.1038/s42255-026-01467-2.

Correspondence and requests for materials should be addressed to Shannon M. Reilly.

Peer review information *Nature Metabolism* thanks the anonymous reviewers for their contribution to the peer review of this work. Primary Handling Editor: Revati Dewal, in collaboration with the *Nature Metabolism* team.

https://doi.org/10.1038/s42255-026-01467-2

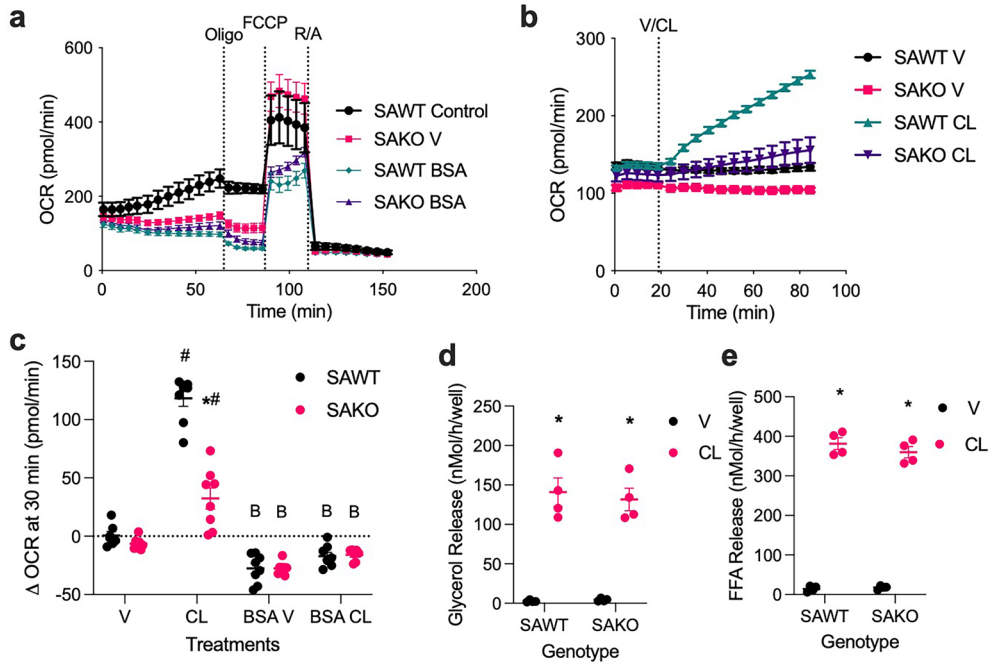

Extended Data Fig. 1 | STAT3 suppresses re-esterification to promote lipolysis driven oxidative metabolism. a and **b**, OCR in male (a) and female (b) primary adipocytes isolated from SAKO and litter mate control SAWT mice. **a**, Treatment times indicated with vertical line for 2 µM oligo, 1 µM FCCP, and 1 µM rotenone/antimycin A (R/A). p-val < 0.05 SAWT V control vs SAWT BSA after 15 min, SAWT V vs SAKO V after 35 min, SAKO V control vs SAKO BSA after 90 min and SAWT V vs SAKO V after 95 min, no significant differences after 110 min. n = 5 SAWT control, 7 SAKO control and 8 BSA wells. **b**, Vehicle or 100 nM CL injected at the indicated time. p-val < 0.05 SAKO CL vs SAKO CL, and SAWT V vs SAWT CL after 25 min. n = 8 wells. **c**, Change in OCR from baseline to 30 min after stimulation with vehicle or 100 nM CL in the presence or absence of 2% BSA in the media. n = 7 V, BSA SAWT, and 8 CL, BSA SAKO wells. *p-val < 0.0001 SAWT vs SAKO, $^{\#}$p-val < 0.0001 V vs CL, ^{A}p-val < 0.0001 + /- BSA. **d** and **e**, the rate of glycerol (d) and FFA (e) release in SAWT and SAKO female primary adipocytes treated with vehicle or 100 nM CL. *p-val < 0.0001 V vs CL. n = 4 wells. Statistical significance determined by two-way ANOVA with Holm-Sidak post-hoc to adjust for multiple comparisons, exact p-values for all comparisons included in source data[68]. Data are presented as mean ± SEM.

https://doi.org/10.1038/s42255-026-01467-2

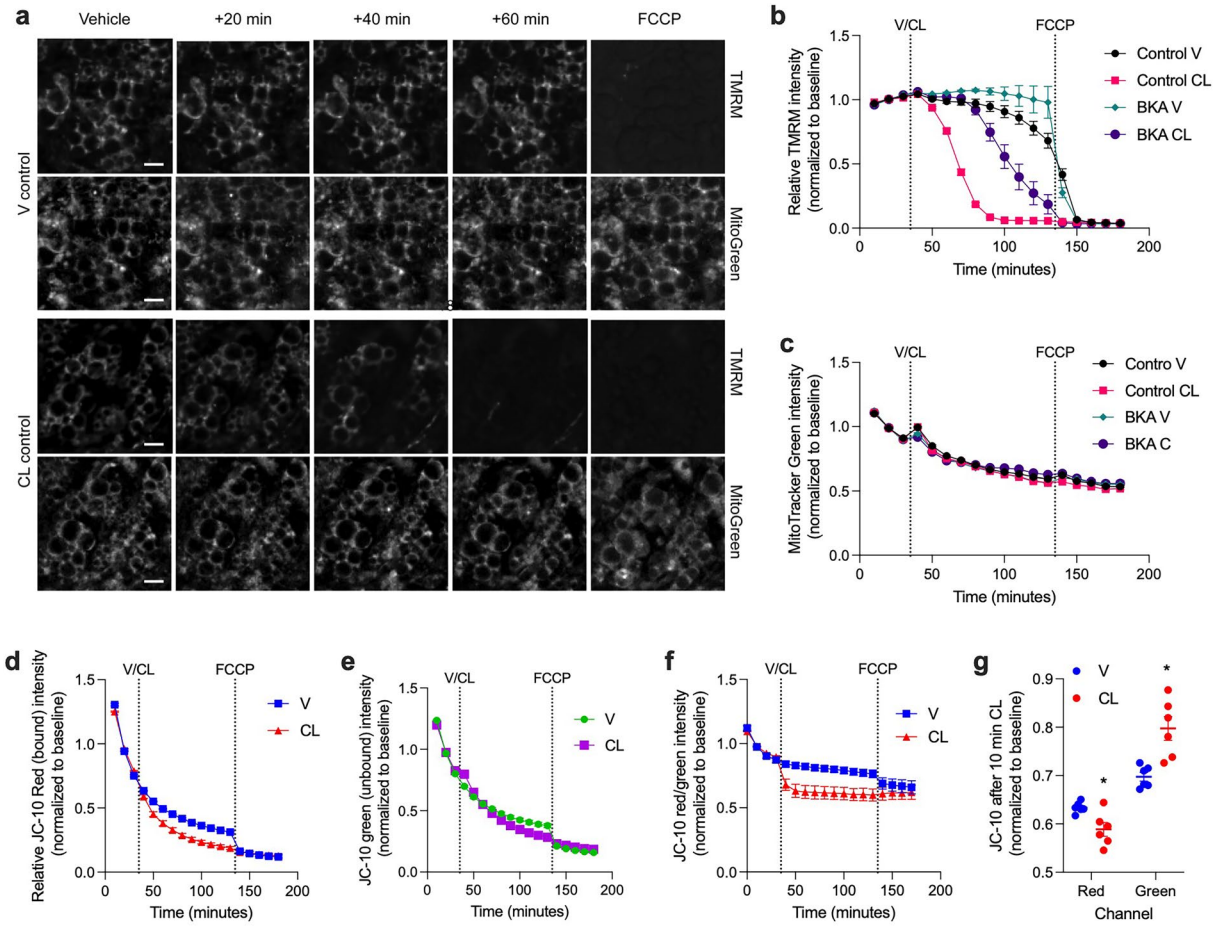

Extended Data Fig. 2 | Imaging mitochondrial membrane potential. Imaging in male primary adipocytes at baseline and after treatment with 100 nM CL-316,243 or vehicle, and finally 1 µM FCCP. **a**, Representative TMRM and MitoGreen micrographs. After baseline images were collected, 100 nM CL-316,243 or vehicle was added at time zero and imaging continued. The last image was taken after the addition of 1 µM FCCP. Scale bar = 20 µm. **b** and **c**, Baseline normalized TMRM (b) and Mitogreen (c) staining in male primary adipocytes pretreated with 50 µM BKA or V. n = 6 wells. **b**, p-val < 0.05 control V vs control CL and control CL vs BKA CL from 60 min, BKA V vs BKA CL from 80 min, and Control V vs BKA V from 90 min, no significant differences observed after FCCP treatment. **d-f**, Baseline normalized 15 µM JC10 red (d), green (e) and red/green (f) staining. p-val < 0.0001 V vs CL 50-130 min (d) and 40, 80-130 min (e). p-val < 0.05 V vs CL 40-130 min (f). n = 6 wells. **g**, JC10 staining intensity in both red and green channels 10 min after CL relative to baseline. *p-val < 0.05 V vs CL. n = 6 wells. Statistical significance determined by two-way ANOVA with Holm-Sidak post-hoc to adjust for multiple comparisons, exact p-values for all comparisons included in source data[68]. Data are presented as mean ± SEM.

https://doi.org/10.1038/s42255-026-01467-2

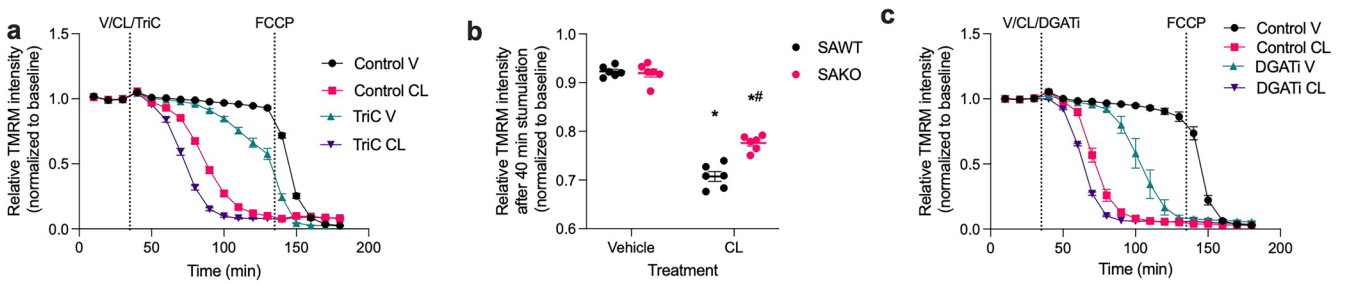

Extended Data Fig. 3 | Re-esterification antagonizes mitochondrial depolarization. a, Baseline normalized TMRM staining in female primary adipocytes stimulated with 5 µM Triacsin C (TriC) or control, and 100 nM CL or V and FCCP treatments at indicated timepoints. p-val < 0.05 Control V vs Control CL from 60 min to 160 min, TriC V vs TriC CL from 50 min to 120 min, Control CL vs TriC CL from 60 min, Control V vs TriC V from 90 min. n = 6 wells. **b**, Baseline normalized TMRM staining in male primary adipocytes 40 min after stimulation with V or 100 nM CL. *p-val < 0.0001 V vs CL, $^{\#}$p-val < 0.0001 SAWT vs SAKO. n = 6 wells. **c**, Baseline normalized TMRM staining in female primary adipocytes stimulated with 10 µM DGATi or Control +/- 100 nM CL and then FCCP treatments at indicated timepoints. p-val < 0.05 Control V vs Control CL, DGATi V vs DGATi CL and Control CL vs DGATi CL from 60 min. p-val < 0.05 Control V vs DGATi V from 90 min. n = 6 control and 3 DGATi wells. No significant differences observed in last 30 min of FCCP treatment. Statistical significance determined by two-way ANOVA with Holm-Sidak post-hoc to adjust for multiple comparisons, exact p-values for all comparisons included in source data[68]. Data are presented as mean ± SEM.

https://doi.org/10.1038/s42255-026-01467-2

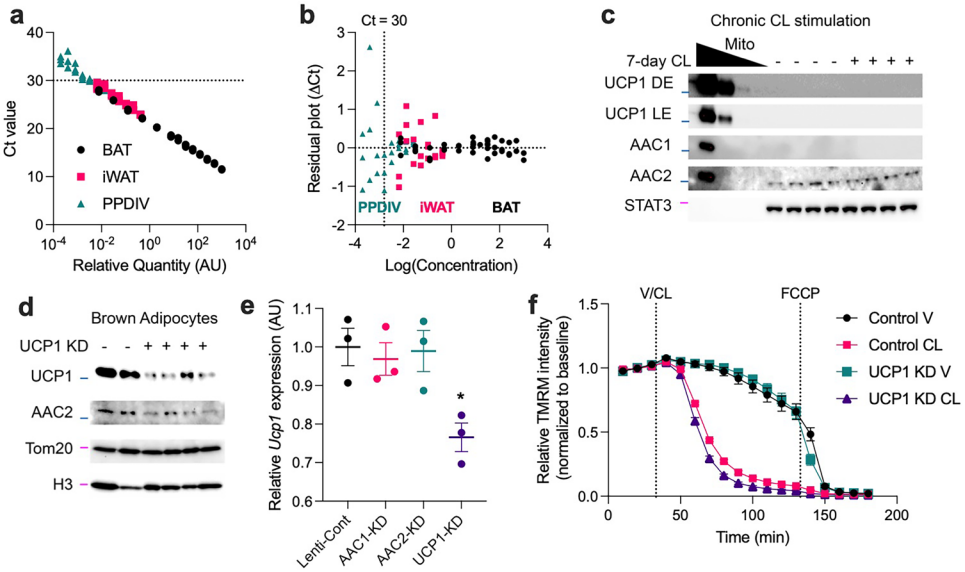

Extended Data Fig. 4 | Ucp1 expression is not detectable in primary adipocytes, nor does it impact uncoupling. a, Cycle threshold values of standards from indicated samples. **b**, Residual plot of linear regression of data in panel A. **c**, Western Blot of female primary adipocytes with and without 7-day CL treatment. The first 3 lines are a serial ten-fold dilution of mitochondrial protein fraction from BAT, except AAC1 which is heart mitochondrial protein. Dark exposure (DE), Light exposure (LE). Blue: 25 kDa, pink: 100 kDa size markers. UCP1, AAC1 and AAC2 were run in parallel on separate gels with the same samples, STAT3 blot was from the same gel as UCP1, and is representative of loading controls from AAC gels. **d**, Western Blot in male primary brown adipocytes treated with control, UCP1-1 (lanes 3 and4), and UCP1-2 (lanes 5 and 6) knock down (KD) lentivirus. Blue-25 kDa, pink-15 kDa size markers. UCP1/TOM20 blots and AAC2/H3 blots were from the same gel, the two gels were run in parallel with the same samples. Blots in c and d are representative of multiple experiments. **e**, Relative UCP1 expression in male primary adipocytes treated with indicated KD lentiviruses. *p-val = 0.02 Control vs UCP1 KD. **f**, Relative TMRM intensity in UCP1 KD and control male primary adipocytes stimulated with 100 nM CL or vehicle. p-val < 0.0001 Control V vs Control CL and UCP1 KD V vs UCP1 KD CL from 60 min. p-val < 0.05 Control CL vs UCP1 KD CL 60-80 min. No significant differences observed after 10 min FCCP. n = 6 wells. Statistical significance determined by one-way (e) or two-way (f) ANOVA with Holm-Sidak post-hoc to adjust for multiple comparisons, exact p-values for all comparisons included in source data[68]. Data are presented as mean ± SEM.

https://doi.org/10.1038/s42255-026-01467-2

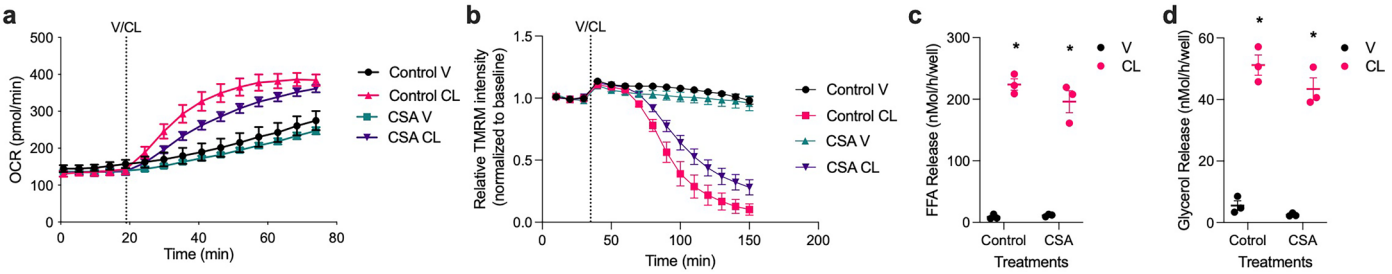

Extended Data Fig. 5 | CSA slightly attenuates uncoupled respiration in lipolytic adipocytes. a, OCR in male primary adipocytes pretreated with 50 mg/mL Cyclosporin A (CSA) or control for 24 h, then stimulated with 100 nM CL or V in port A. p-val < 0.05 Control V vs Control CL after 25 min, CSA V vs CSA CL after 30 min, and Control CL vs CSA CL 35-60 min. n = 3 Control V, 4 CSA V, 6 Control CL and 5 CSA CL wells. **b**, Baseline normalized TMRM staining in female primary adipocytes pretreated with 50 mg/mL CSA or control for 24 h and stimulated with 100 nM CL or V. p-val < 0.05 Control V vs Control CL from 80 min, CSA V vs CSA CL and Control CL vs CSA CL from 90 min, Control V vs CSA V not significantly different. n = 6 wells. **c** and **d**, the rate of FFA (c) and glycerol (d) release in male primary adipocytes pretreated with vehicle or 50 mg/mL CSA or V for 24 h, then 100 nM CL. *p-val < 0.0001 V vs CL. n = 3 wells. Statistical significance determined by two-way ANOVA with Holm-Sidak post-hoc to adjust for multiple comparisons, exact p-values for all comparisons included in source data[68]. Data are presented as mean ± SEM.

https://doi.org/10.1038/s42255-026-01467-2

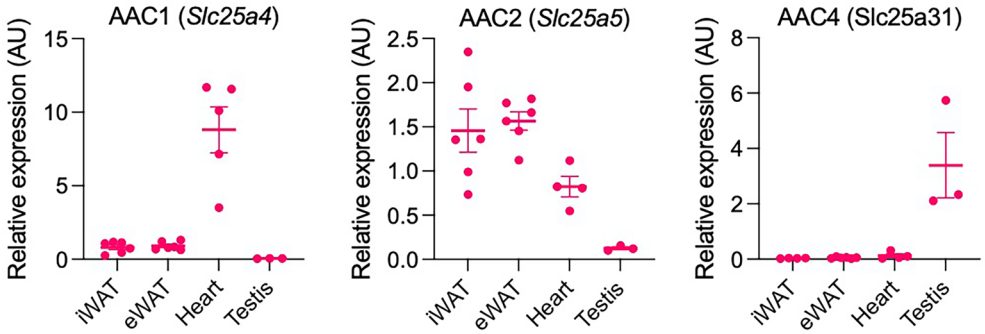

Extended Data Fig. 6 | AAC isoform expression in mice. Expression of AAC isoforms was assessed in isolated tissues from HFD fed male mice housed at 30 °C for a month. iWAT and eWAT n = 6 mice, heart n = 4 mice, and testis n = 3 mice. *p-val < 0.05 vs other tissues. AAC1: p-val < 0.0001 Heart vs iWAT, Heart vs eWAT, and Heart vs Testis. AAC2: p-val = 0.001 iWAT vs Testis, 0.0006 eWAT vs Testis, and 0.04 eWAT vs Heart. AAC4: p-val = 0.0005 Testis vs iWAT, 0.0003 Testis vs eWAT, and 0.0007 Testis vs Heart. Statistical significance determined by one-way ANOVA with Holm-Sidak post-hoc to adjust for multiple comparisons. Data are presented as mean ± SEM.

https://doi.org/10.1038/s42255-026-01467-2

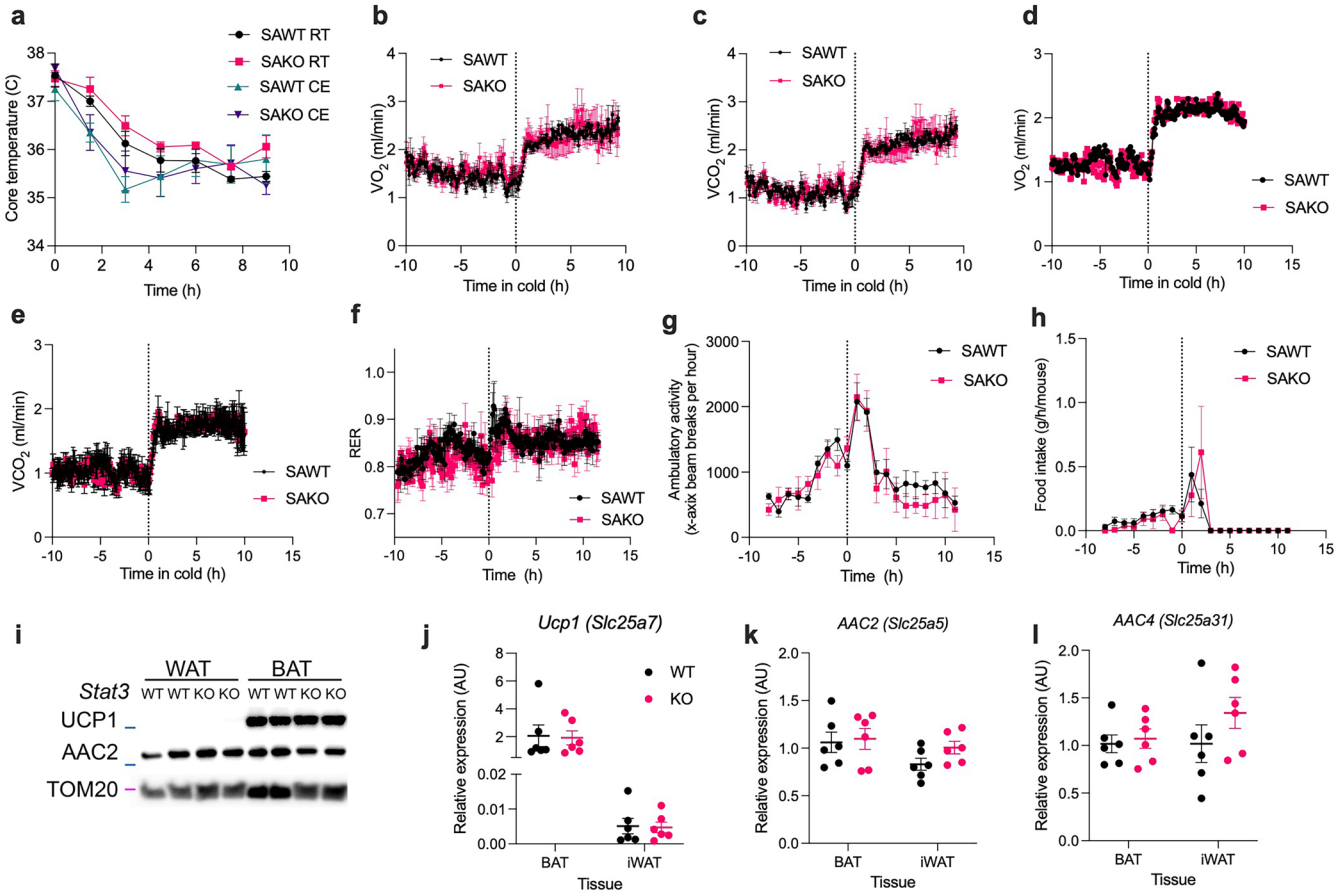

Extended Data Fig. 7 | Cold sensitivity in SAWT and SAKO. a, Core body temperature during acute cold exposure (CE) or room temperature controls (RT) in normal diet fed male SAKO and SAWT mice. No statistically significance differences observed between genotypes. n = 10 mice. **b** and **c**, VO2 (b) and VCO2 (c) of normal diet fed male SAWT and SAKO mice at 30 °C then transitioned to 5 °C (cold) at time zero. n = 5 mice. **d** and **e**, VO2 (d) and VCO2 (e) of normal diet fed female SAWT and SAKO mice at 30 °C then transitioned to 5 °C (cold) at time zero. n = 5 mice. **f - h**, Respiratory exchange ratio (f), ambulatory activity (g), and food intake (h) in obese thermoneutral adapted male SAWT and SAKO mice at 30 °C then transitioned to cold at time zero. n = 10 SAWT and 5 SAKO mice. **i**, UCP1 and AAC2 protein expression in mitochondrial fractions isolated from BAT and iWAT of obese, thermoneutral-adapted female SAKO and SAWT mice. n = 2 mice. Blue-25 kDa, pink-15 kDa size markers. UCP1 and AAC2 blots were run in parallel on separate gels with the same samples, TOM20 blot was from the same gel as UCP1, and is representative TOM20 from the AAC2 gel. **j-l**, mRNA expression levels of Ucp1 (j), AAC2 (k), and Gpr3 (l) were assessed in iWAT and BAT isolated from obese, thermoneutral-adapted male SAKO and SAWT mice. n = 6 mice. Statistical significance determined by two-way ANOVA with Holm-Sidak post-hoc to adjust for multiple comparisons, exact p-values for all comparisons included in source data[68]. Data are presented as mean ± SEM.

https://doi.org/10.1038/s42255-026-01467-2

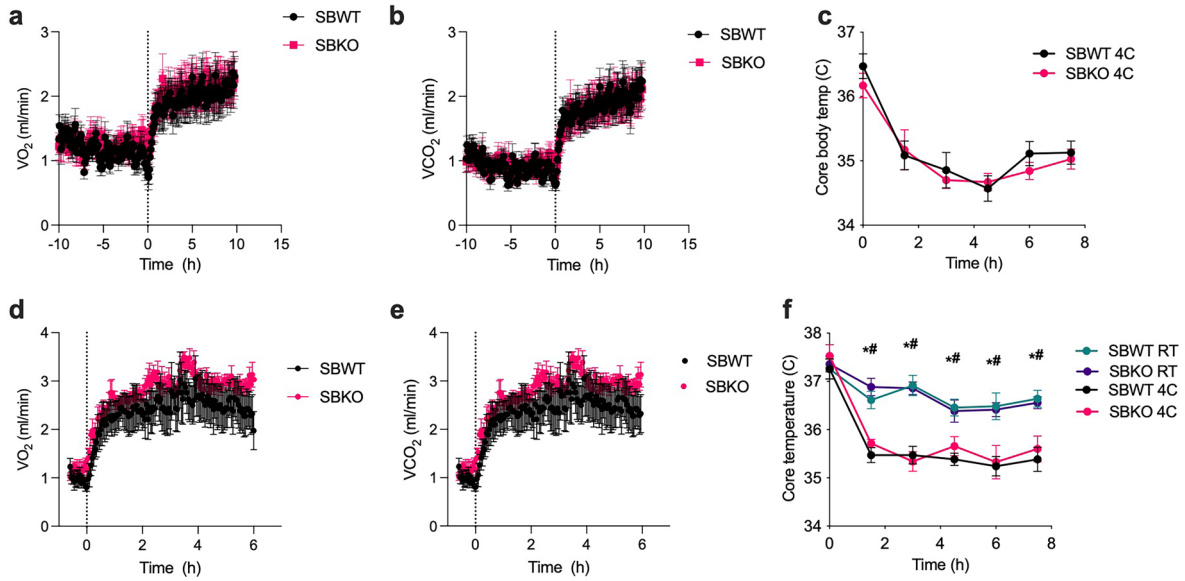

Extended Data Fig. 8 | SBKO mice do not exhibit cold sensitivity relative to SBWT controls. a, and **b**, VO_2 (a) and VCO_2 (b) of normal diet fed male SBWT and SBKO mice at housed 30 °C and transitioned to 5 °C (cold) at time zero. n = 7 SBWT and 8 SBKO. **c**, Acute cold exposure in obese thermoneutral adapted male SBWT and SBKO mice. n = 7 mice. **d** and **e**, VO_2 (d) and VCO_2 (e) of obese thermoneutral adapted male SBWT and SBKO mice at 30 °C then transitioned to 5 °C (cold) at time zero. n = 4 mice. **f**, Acute cold exposure in obese thermoneutral adapted female SBWT and SBKO mice with room temperature controls. n = 7 mice. *p-val < 0.05 SBWT RT vs SBWT 4 C, #p-val < 0.05 SBKO RT vs SBKO 4 C. SBWT vs SBKO not significantly different at any time. Statistical significance determined by two-way ANOVA with Holm-Sidak post-hoc to adjust for multiple comparisons, exact p-values for all comparisons included in source data[68]. Data are presented as mean ± SEM.

https://doi.org/10.1038/s42255-026-01467-2

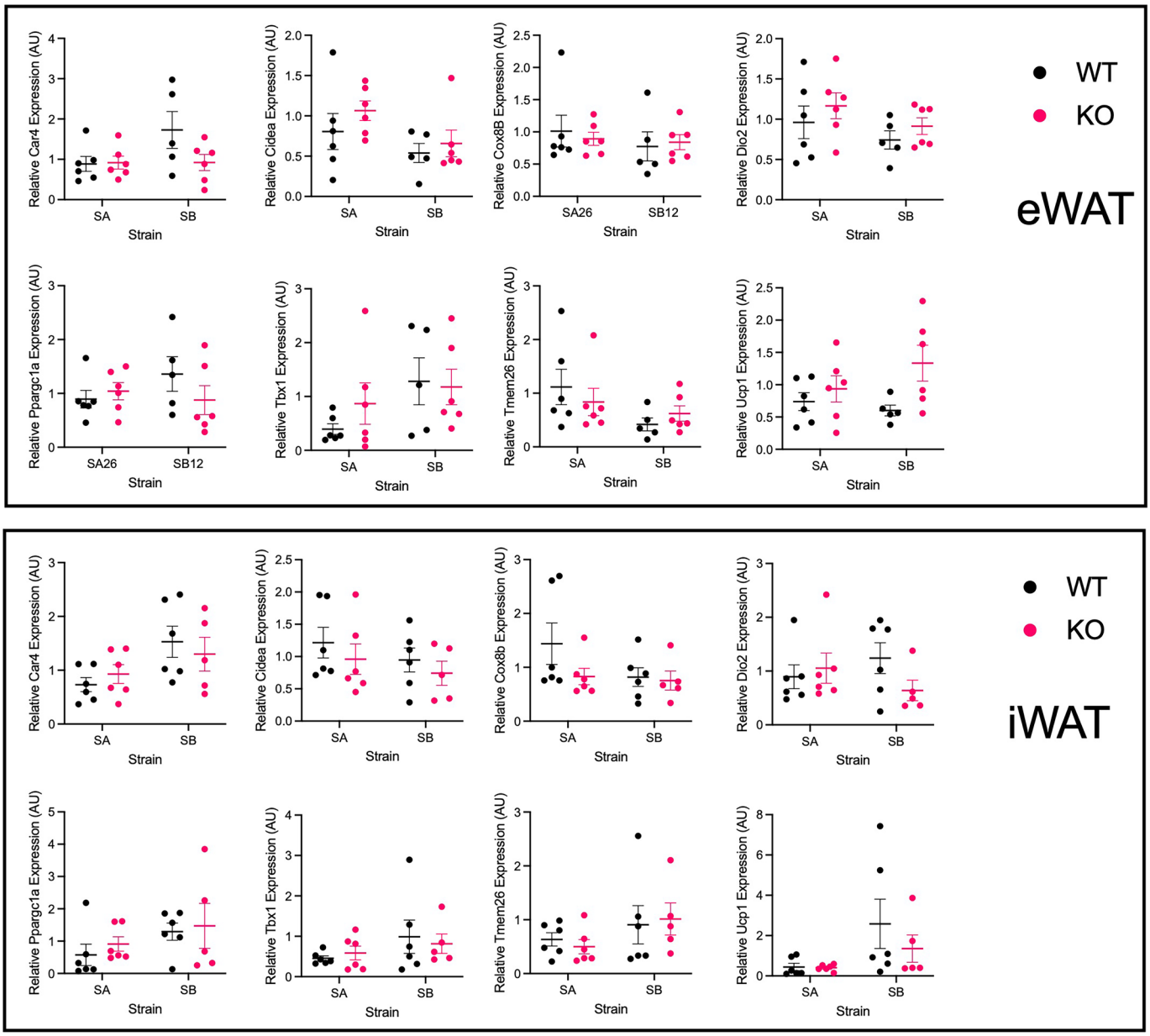

Extended Data Fig. 9 | Gene expression in Stat3 Knockout adipose tissues. Expression of various brown/beige associated genes in inguinal and epididymal white adipose tissue. No statistically significant changes in gene expression were observed. n = 6 mice, except SBWT eWAT and SBKO iWAT n = 5 mice. Statistical significance determined by two-way ANOVA with Holm-Sidak post-hoc to adjust for multiple comparisons, exact p-values for all comparisons included in source data[68]. Data are presented as mean ± SEM.

https://doi.org/10.1038/s42255-026-01467-2

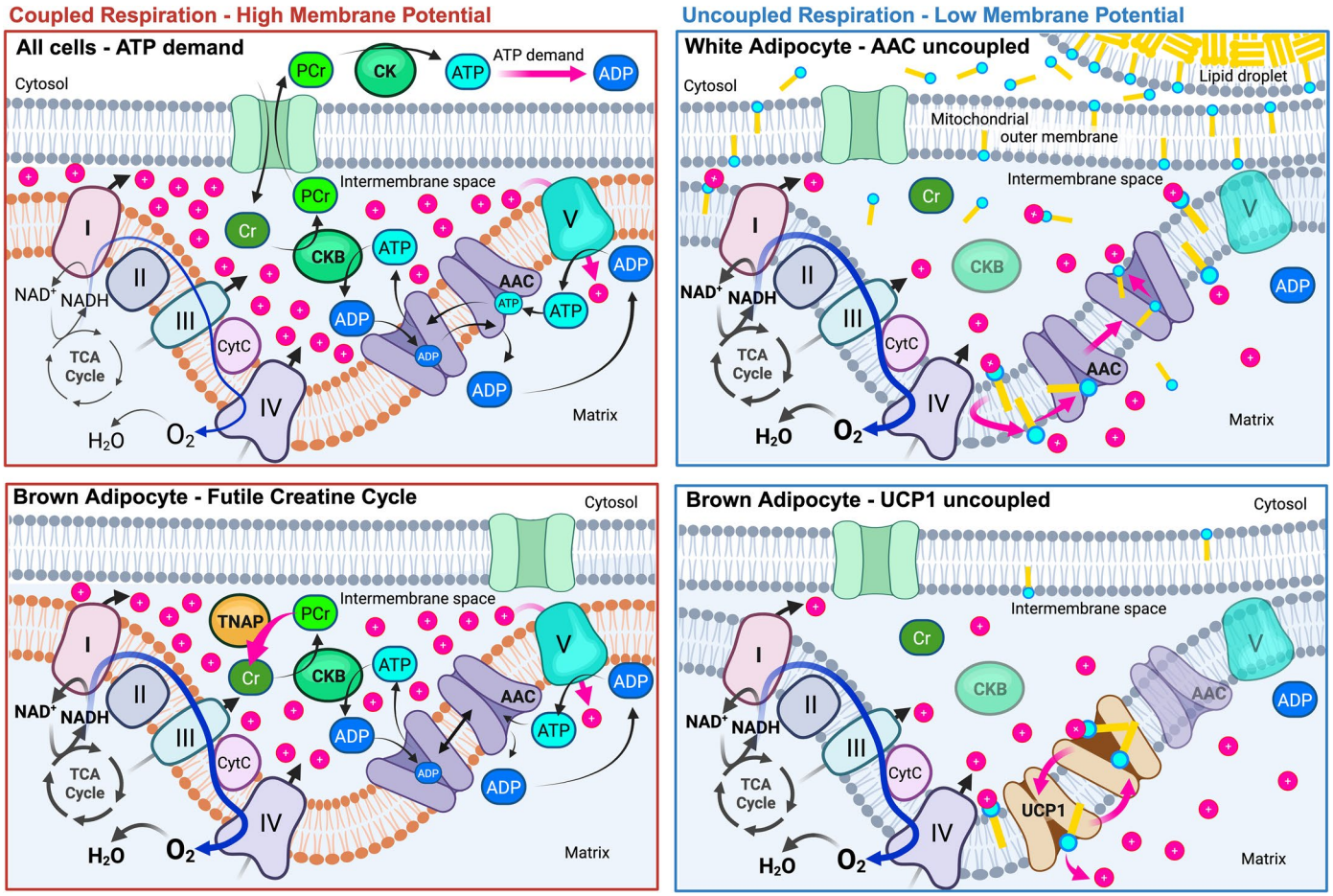

Extended Data Fig. 10 | Models of different types of coupled and uncoupled respiration. Two models of coupled respiration are shown on the left. Coupled respiration maintains a high mitochondrial membrane potential to generate the proton motive force that drives ATP synthesis. The upper left panel depicts conventional coupled respiration, which can be thermogenic when ATP is consumed by futile cycles such as triglyceride or calcium cycling. The lower left panel illustrates creatine futile cycling which, although coupled, is intrinsically thermogenic due to tissue-nonspecific alkaline phosphatase (TNAP) activity in the mitochondrial intermembrane space. Two models of uncoupled respiration are shown on the right. The lower right panel depicts UCP1-mediated uncoupling in brown adipocytes which is notably independent of the ATP/ADP carrier (AAC). The upper right panel illustrates AAC-mediated uncoupling in white adipocytes, which requires elevated free fatty acid levels generated during active lipolysis. Fatty acid–binding proteins facilitate cytosolic trafficking of free fatty acids, which readily diffuse across membranes and undergo protonated flip-flop transport. Created using BioRender.com.

nature portfolio

Corresponding author(s): Shannon M. Reilly

Last updated by author(s): Dec 27, 2025

Reporting Summary

Nature Portfolio wishes to improve the reproducibility of the work that we publish. This form provides structure for consistency and transparency in reporting. For further information on Nature Portfolio policies, see our Editorial Policies and the Editorial Policy Checklist.

Statistics

For all statistical analyses, confirm that the following items are present in the figure legend, table legend, main text, or Methods section.

n/a	Confirmed	
☐	☒	The exact sample size (*n*) for each experimental group/condition, given as a discrete number and unit of measurement
☐	☒	A statement on whether measurements were taken from distinct samples or whether the same sample was measured repeatedly
☐	☒	The statistical test(s) used AND whether they are one- or two-sided *Only common tests should be described solely by name; describe more complex techniques in the Methods section.*
☐	☒	A description of all covariates tested
☐	☒	A description of any assumptions or corrections, such as tests of normality and adjustment for multiple comparisons
☐	☒	A full description of the statistical parameters including central tendency (e.g. means) or other basic estimates (e.g. regression coefficient) AND variation (e.g. standard deviation) or associated estimates of uncertainty (e.g. confidence intervals)
☐	☒	For null hypothesis testing, the test statistic (e.g. *F*, *t*, *r*) with confidence intervals, effect sizes, degrees of freedom and *P* value noted *Give P values as exact values whenever suitable.*
☒	☐	For Bayesian analysis, information on the choice of priors and Markov chain Monte Carlo settings
☒	☐	For hierarchical and complex designs, identification of the appropriate level for tests and full reporting of outcomes
☒	☐	Estimates of effect sizes (e.g. Cohen's *d*, Pearson's *r*), indicating how they were calculated

Our web collection on statistics for biologists contains articles on many of the points above.

Software and code

Policy information about availability of computer code

Data collection	Data from metabolic cages was collected using the Promethion Live software by Sable Systems
Data analysis	The data was processed using Macros13 provided by Sable Systems, then visualized in Prism.

For manuscripts utilizing custom algorithms or software that are central to the research but not yet described in published literature, software must be made available to editors and reviewers. We strongly encourage code deposition in a community repository (e.g. GitHub). See the Nature Portfolio guidelines for submitting code & software for further information.

Data

Policy information about availability of data

All manuscripts must include a data availability statement. This statement should provide the following information, where applicable:

- Accession codes, unique identifiers, or web links for publicly available datasets
- A description of any restrictions on data availability
- For clinical datasets or third party data, please ensure that the statement adheres to our policy

The experimental data and statistical analyses that support the findings of this study are available in FigShare with the identifier: https://doi.org/10.6084/m9.figshare.27022276

Research involving human participants, their data, or biological material

Policy information about studies with human participants or human data. See also policy information about sex, gender (identity/presentation), and sexual orientation and race, ethnicity and racism.

Reporting on sex and gender	*Use the terms sex (biological attribute) and gender (shaped by social and cultural circumstances) carefully in order to avoid confusing both terms. Indicate if findings apply to only one sex or gender; describe whether sex and gender were considered in study design; whether sex and/or gender was determined based on self-reporting or assigned and methods used.* *Provide in the source data disaggregated sex and gender data, where this information has been collected, and if consent has been obtained for sharing of individual-level data; provide overall numbers in this Reporting Summary. Please state if this information has not been collected.* *Report sex- and gender-based analyses where performed, justify reasons for lack of sex- and gender-based analysis.*
Reporting on race, ethnicity, or other socially relevant groupings	*Please specify the socially constructed or socially relevant categorization variable(s) used in your manuscript and explain why they were used. Please note that such variables should not be used as proxies for other socially constructed/relevant variables (for example, race or ethnicity should not be used as a proxy for socioeconomic status).* *Provide clear definitions of the relevant terms used, how they were provided (by the participants/respondents, the researchers, or third parties), and the method(s) used to classify people into the different categories (e.g. self-report, census or administrative data, social media data, etc.)* *Please provide details about how you controlled for confounding variables in your analyses.*
Population characteristics	*Describe the covariate-relevant population characteristics of the human research participants (e.g. age, genotypic information, past and current diagnosis and treatment categories). If you filled out the behavioural & social sciences study design questions and have nothing to add here, write "See above."*
Recruitment	*Describe how participants were recruited. Outline any potential self-selection bias or other biases that may be present and how these are likely to impact results.*
Ethics oversight	*Identify the organization(s) that approved the study protocol.*

Note that full information on the approval of the study protocol must also be provided in the manuscript.

Field-specific reporting

Please select the one below that is the best fit for your research. If you are not sure, read the appropriate sections before making your selection.

☒ Life sciences ☐ Behavioural & social sciences ☐ Ecological, evolutionary & environmental sciences

For a reference copy of the document with all sections, see nature.com/documents/nr-reporting-summary-flat.pdf

Life sciences study design

All studies must disclose on these points even when the disclosure is negative.

Sample size	Sample sizes for animal experiments were determined by power analysis (0.8) using an estimated effect size from preliminary experiments. Sometimes sample sizes were limited by random variation in litter size and/or genotype distribution resulting in less than the ideal number of animals born within a 4 week span. Sample size in seahorse experiments was 6 to 8-wells, while imaging experiments used a sample size of 6-wells, so that all groups in an experiment were run on the same 96-well plate with cell free wells for background correction.
Data exclusions	Wells in which the adipocytes had become detached, or differentiation rates were under 90% were identified visually and omitted from the analysis.
Replication	Results were replicated in at least three separate experiments.
Randomization	Within each genotype, mice were assigned to treatment groups, such that prior to treatment the mean body weight, as well as the standard deviation of the body weight, was equal across treatment groups, using a method similar to block randomization. Additional consideration was given to housing, such that each cage contained multiple treatment groups, to avoid confounding by cage effects.
Blinding	During animal studies, ear tags were used to identify animals. Researchers performing tests and collecting data were blinded during experiments.

Reporting for specific materials, systems and methods

We require information from authors about some types of materials, experimental systems and methods used in many studies. Here, indicate whether each material, system or method listed is relevant to your study. If you are not sure if a list item applies to your research, read the appropriate section before selecting a response.

Materials & experimental systems

n/a	Involved in the study
☐	☒ Antibodies
☐	☒ Eukaryotic cell lines
☒	☐ Palaeontology and archaeology
☐	☒ Animals and other organisms
☒	☐ Clinical data
☒	☐ Dual use research of concern
☒	☐ Plants

Methods

n/a	Involved in the study
☒	☐ ChIP-seq
☒	☐ Flow cytometry
☒	☐ MRI-based neuroimaging

Antibodies

Antibodies used

The following antibodies were used for western blotting: AAC2 (Cell Signaling, Cat: 14671, clone: E2B9D, lot: 1), Histone H3 (Cell Signaling, Cat: 4499, clone: D1H2, lot: 20), STAT3 (Cell Signaling, Cat: 9139, clone: 124H6, lot: 16), TOM20 (Cell Signaling, Cat: 42406, clone: D8T4N, lot: 4), UCP1 (Cell Signaling, Cat: 72298, clone: E9C2V, lot: 3), AAC1 (Thermo Fisher, Cat: MA5-55372, clone: 1U7X1, lot: 2K4533001C), Goat anti-mouse IgG (H+L) (Thermo Fisher, Cat: 31430, lot: YF375332), Goat anti-rabbit IgG (H+L) (Thermo Fisher, Cat: 31460, lot: 33)

Validation

Primary antibodies were validated by the manufacturer and confirmed in the lab by western blot using knockout (STAT3), knockdown (AAC2), tissue specificity (AAC1, UCP1) or subcellular fractionation (H3, TOM20).
AAC2 specificity was confirmed by western blot of extracts from various cells lines: https://www.cellsignal.com/products/primary-antibodies/ant2-slc25a5-e2b9d-rabbit-monoclonal-antibody/14671
H3 specificity was confirmed by western blot of extracts from various cells lines not to cross-react with other core histones: https://www.cellsignal.com/products/primary-antibodies/histone-h3-d1h2-rabbit-monoclonal-antibody/4499
STAT3 specificity was confirmed by western blot of extracts from various cells lines and mouse tissues: https://www.cellsignal.com/products/primary-antibodies/stat3-124h6-mouse-monoclonal-antibody/9139
TOM20 specificity was confirmed by western blot of extracts from various cells lines: https://www.cellsignal.com/products/primary-antibodies/tom20-d8t4n-rabbit-monoclonal-antibody/42406
UCP1 specificity was confirmed by western blot of mouse BAT and liver (negative control): https://www.cellsignal.com/products/primary-antibodies/ucp1-e9z2v-rabbit-monoclonal-antibody/72298
AAC1 specificity was confirmed by western blot of WT and KO samples: https://www.thermofisher.com/antibody/product/ANT-Antibody-clone-1U7X1-Recombinant-Monoclonal/MA5-55372 (Figure 2)

Secondary antibodies were validated by the manufacturer.
Specificity of the Goat anti-mouse secondary antibody was confirmed by western blot of purified Mouse IgG, Mouse IgG1, Mouse IgG2a, Mouse IgG2b, Mouse IgG3, Mouse IgM, Rabbit IgG, Goat IgG, Chicken IgY, Rat IgG, Human IgG proteins. https://www.thermofisher.com/antibody/product/Goat-anti-Mouse-IgG-H-L-Secondary-Antibody-Polyclonal/31430 (Figure 4)
Specificity of the Goat anti-rabbit secondary antibody was confirmed by western blot. https://www.thermofisher.com/antibody/product/Goat-anti-Rabbit-IgG-H-L-Secondary-Antibody-Polyclonal/31460

Eukaryotic cell lines

Policy information about cell lines and Sex and Gender in Research

Cell line source(s)

3T3-L1 cells were originally purchased from American Type Culture Collection by Alan R Saltiel.

Authentication

3T3-L1 cells were validated by American Type Culture Collection, and also by functionality in the Reilly and Saltiel Labs for efficient adipogenesis.

Mycoplasma contamination

All cell lines tested negative for mycoplasma in routine tests.

Commonly misidentified lines
(See ICLAC register)

No commonly misidentified cell lines were used.

Animals and other research organisms

Policy information about studies involving animals; ARRIVE guidelines recommended for reporting animal research, and Sex and Gender in Research

Laboratory animals

Male and female C57BL/6J mice from 2 to 12 months of age were used in this study.

Wild animals

The study did not involve wild animals.

Reporting on sex

Experiments were performed in male and female cohorts separately.. Direct comparison between sexes was not performed due to confounding by metabolic differences in adiposity that caused the sexes to be analyzed at different ages. The main effect was observed in both sexes. Cellular sex is also reported for experiment performed in primary cells.

Field-collected samples	The study did not involve samples collected from the field.
Ethics oversight	All animal use was approved by the Institutional Animal Care and Use Committee (IACUC) at Weill Cornell Medicine

Note that full information on the approval of the study protocol must also be provided in the manuscript.

Plants

Seed stocks	*Report on the source of all seed stocks or other plant material used. If applicable, state the seed stock centre and catalogue number. If plant specimens were collected from the field, describe the collection location, date and sampling procedures.*
Novel plant genotypes	*Describe the methods by which all novel plant genotypes were produced. This includes those generated by transgenic approaches, gene editing, chemical/radiation-based mutagenesis and hybridization. For transgenic lines, describe the transformation method, the number of independent lines analyzed and the generation upon which experiments were performed. For gene-edited lines, describe the editor used, the endogenous sequence targeted for editing, the targeting guide RNA sequence (if applicable) and how the editor was applied.*
Authentication	*Describe any authentication procedures for each seed stock used or novel genotype generated. Describe any experiments used to assess the effect of a mutation and, where applicable, how potential secondary effects (e.g. second site T-DNA insertions, mosiacism, off-target gene editing) were examined.*